Chemical Engineering Journal 527 (2026) 171357

Contents lists available at ScienceDirect

Chemical Engineering Journal

journal homepage: www.elsevier.com/locate/cej

Degrees of rate control and AutoDiff-driven direct sensitivity analysis in heterogeneous catalysis

Olajide H. Bamidele [a,1], Sina Behtash [a,1], Mubarak Bello [a], Andreas Heyden [a,*]

[a] Department of Chemical Engineering, University of South Carolina, Columbia, SC, 29208, USA

ARTICLE INFO

Keywords:
DRC
Transient DRC
Automatic differentiation
Sensitivity analysis
Microkinetic modeling
Finite difference

ABSTRACT

Despite the wide application and benefits of the degree of rate control (DRC) analysis, several details remain argued, particularly about the conservation of DRCs at transient (TR) and steady-state (SS) conditions, especially for complex reaction networks. This work argues that previous proofs about the conservation properties of DRCs have been incomplete, and we provide new mathematical proofs at TR and SS conditions. In addition, we use both analytical (automatic differentiation) and numerical (finite difference) approaches to compute DRCs for the case study of ethane hydrogenolysis (EH) over Pt(111). This work confirms that at both TR and SS conditions, the sum of all DRCs, i.e., sum of the degrees of kinetic (DKRC) and thermodynamic rate control (DTRC), is conserved at zero. At SS conditions, the sum of DKRC is conserved at 1 while the sum of DTRC is conserved at −1. In corroboration of previous works, we show that the DTRC for any adsorbate at SS is equal to the product of the species coverage and a constant. In contrast, at TR conditions, the individual sums of both DTRC and DKRC are not conserved and can be any real number, with potential implications for the novel field of dynamic catalysis. Finally, we show that the conventional finite difference (FD) approach, only useful at SS, is prone to inaccuracy and very sensitive to the value of the differential change applied. The optimal differential value also varies significantly with system and rate definition. Consequently, we describe and illustrate in this work the application of the automatic differentiation (AD) approach for the more accurate determination of DRCs at both TR and SS conditions.

1. Introduction

First-principles modeling of most chemical processes typically results in a multistep reaction mechanism. One aim of chemical kinetics studies is to unravel the complex relationship between the overall rate of a reaction process and the energetics of all species—intermediates and transition states—involved in its mechanism. Usually, more than one elementary step and surface intermediate have significant influence on the net reaction rate. Hence, selectively modifying such species' stability (i.e., its free energy), either by external fields, catalyst modification, or solvent selection could greatly improve the overall reaction rate [1,2]. Therefore, identifying such elementary steps, commonly referred to as the rate-controlling steps and intermediates, is crucial. We note here that Kozuch and Martin [3] advocate the use of the term rate-determining or rate-controlling "state" instead of rate-determining or rate-controlling "step" since what is typically meant is the transition state of the rate-controlling step and not a combination of the reactant, product, and transition state. While we agree with Kozuch and Martin, we will nevertheless use the term rate-controlling step as it is common in the heterogeneous catalysis literature.

Various works have been done to assess which steps and intermediates in a reaction scheme limit the overall rate. Christiansen [4], in one of the earliest pivotal works aimed at understanding the reaction mechanism, utilized graph-like diagrams to analyze chemical processes as a series of elementary reactions and obtained reaction turnover frequencies (TOF) by performing linear algebra on the matrix of rate constants [5–7]. However, the complexity of the method and rapid explosion in the number of reaction steps make this approach unattractive for reaction analysis [8]. Boudart [5,9] and Dumesic [10] applied the De Donder relations to demystify the reaction kinetics and mechanism, and Dumesic further posited that rate-determining steps can be identified by mathematical manipulation of the relative affinity for each elementary step. In his response, Campbell [11], who had earlier introduced the concept of "*degree of rate control*" [12], argued that since Dumesic's

* Corresponding author.
E-mail address: heyden@cec.sc.edu (A. Heyden).
[1] Equal contributions.

https://doi.org/10.1016/j.cej.2025.171357
Received 2 September 2025; Received in revised form 18 November 2025; Accepted 27 November 2025
Available online 2 December 2025

affinity expressions do not take any kinetic information of the elementary steps into account—it purely defines a thermodynamic driving force towards equilibrium—it may not be universally applicable in identifying rate-determining step(s) in a reaction scheme. In his rebuttal, Dumesic [13] contended that the De Donder relations are complementary to Campbell's degree of rate control, and he further showed the consistency of the De Donder relations by proving the conservation of sensitivities, obtained in terms of the affinities, to unity. His arguments are later corroborated by Foley and Bhan [14].

To the best of our knowledge, Campbell's degree of rate control is the most widely utilized tool for reaction mechanism analysis and identification of rate-limiting steps. Mathematically, the degree of rate control for elementary reaction step j, $X_{DRC,j|k}$, is defined as the dimensionless partial derivative of the natural log of the overall rate of production of fluid species k, $r_{k,fluid}$ with respect to the natural log of j's forward rate constant, $k_{f,j}$, keeping temperature, fluid phase fugacities/activities, and other rate constants, except the backward rate constant of step j, $k_{b,j}$, constant. Considering that the forward and backward rate constants of any elementary reaction are correlated to the free energy of the transition state via Eyring's transition state theory [7,15], the definition of the $X_{DRC,j|k}$, is then equivalent to taking the partial derivative of the natural log of the overall rate with respect to the dimensionless free energy of the transition state of the step j, while the free energy of all intermediates and other transition states are kept constant [1,16], as shown in eq. 1.

$$X_{DRC,j|k} = \frac{\partial\left(\ln r_{k,fluid}\right)}{\partial\left(\ln k_{f,j}\right)}\bigg|_{k_{f,i\neq j},k_{b,i\neq j},T,P_i} = \frac{\partial\left(\ln r_{k,fluid}\right)}{\partial\left(\frac{-G_j^{\ddagger}}{RT}\right)}\bigg|_{G_{i\neq j}^{\ddagger},G_i^0,T,P_i} \tag{1}$$

Campbell's degree of rate control estimates the influence of a differential change in the free energy of any given transition state on the overall rate of production of species k [11,12,16]. In general, $X_{DRC,j|k}$ is commonly referred to as the degree of kinetic rate control. Without lack of generality, we replaced the activity of fluid species i with its partial pressure, P_i, in eq. 1, as it is common for ideal gases.

In 2006, Kozuch and Shaik [6] applied the concept of the degree of rate control to develop the degree of TOF control, which quantifies the contribution of energy states to the overall reaction rate. In addition, Stegelmann and coworkers extended this concept to the degree of the thermodynamic rate control for intermediates [16], degree of kinetic selectivity control [2], and degree of thermodynamic selectivity control [2]. Similar to the kinetic rate control, the degree of the thermodynamic rate control quantifies the effect of differential change in an intermediate's free energy on the net reaction rate and can be expressed mathematically as:

$$X_{DTRC,i|k} = \frac{\partial\left(\ln r_{k,fluid}\right)}{\partial\left(\frac{-G_i^0}{RT}\right)}\bigg|_{G_i^{\ddagger},G_{j\neq i}^0,T,P_i} \tag{2}$$

Over the decades, these differential sensitivity analyses have been applied in building more representative and accurate microkinetic models that guide endeavors such as catalyst design by iterative screening [17,18], demystification of reaction mechanisms [19–22], and analysis of non(pseudo)steady-state [23] and reversible [24] reaction processes. The evaluation of the degree of rate control in simple reaction networks under idealistic reaction conditions, where the description of the overall rate is simple and analytical derivatives are obtainable, is fairly straightforward. However, for more complex reaction networks and under more realistic reaction conditions without any simplifying assumptions, computation of DRC values is not a trivial task due to the difficulty in obtaining analytical or accurate numerical derivatives.

Dumesic [13], Baranski [21], Shaik [8], and Stegelmann [16] have shown for specific and simple reaction schemes under steady state (SS) conditions that the sum of the degrees of kinetic rate control for all elementary steps in a catalytic cycle is 1. Similarly, Foley and Bhan [14] claim that they have proven that the sum of sensitivities for a generic function is conserved at 1 at SS. They also claim to have proven that the degrees of thermodynamic rate control sum to a negative constant that is equal to the negative of the sensitivity-weighted average of the number of surface species reacting in each step (if the free energies of surface and transition state species is not a function of coverage). Finally, using a similar derivation, they showed that, under transient (TR) conditions, the sum of the degrees of rate control can deviate from 1 [23]. We question the derivations from Foley and Bhan, while we agree with most of their conclusions. One of the objectives of this paper is to illustrate why we disagree with previous proofs and provide a new proof that, at SS, the degrees of kinetic rate control sum to 1, while the degrees of thermodynamic rate control sum to negative (−1). Under TR conditions, the overall sum of kinetic and thermodynamic rate controls is conserved at zero, although the sum of kinetic rate controls can become a very large number under TR conditions.

In practice, most of the DRC evaluations are performed numerically by using the finite difference (FD) method [11]. Approximation of differentials by FD is performed by correlating the response of the target model to the measured perturbation in input parameter. As in the case for all FD applications, the size of perturbation in input parameter must be shrewdly chosen such that it is small enough to invoke a linear response in the model output and not too small to prevent errors due to loss of precision [25–27]. Computational intensive methods such as the direct sensitivity analysis and the adjoint sensitivity analysis eliminate the need for perturbations [28]. While the former involves the solution of a composite model encompassing the original model equations and variational equations, i.e., differential equations of the state variables with respect to parameters of interest, the latter involves the integration of a function of an adjoint variable and a carefully defined scalar functional [26,28–30]. Although, these two methods are expected to yield accurate sensitivity values, the high computational requirement and complexity associated with the evaluation of vectors and tensors of differential elements, such as the model Jacobian and Hessian, has limited their application in catalysis studies, where models of real chemical processes can be significantly large. However, the advent of symbolic differentiation and automatic differentiation (AD) algorithms makes the computation of these derivatives possible and memory efficient [25,28]. Although, they did not use either of the two methods, Yang et al. [26] pioneered the application of automatic differentiation to evaluate degrees of rate control in representative reaction models. Specifically, they computed the kinetic DRC values using the forward mode AD and showed its superiority at evaluating accurate sensitivities compared to the FD method. In contrast, this work utilizes the direct sensitivity analysis technique coupled with reverse mode AD-derived differentials to compute both thermodynamic and kinetic DRC values.

We highlight that, with advances in dynamic catalysis, programmable catalysts have the potential to decouple successive elementary reaction steps via controlled external stimuli such as resonance frequency [31], modulating electric or magnetic fields [32–34], surface strains and illumination [35], which selectively alters adsorbate and TS

binding energies. By selectively changing species binding energies, product turnover frequencies and selectivity can be enhanced beyond the theoretical Sabatier maximum and equilibrium limits [31,36–41]. Transient DRC evaluation of complex reaction systems with such instantaneous changes on the time scale of the reaction can only be accurately computed with analytical methods such as the AD technique, as FD techniques often struggle to capture such dynamics [31]. Identification of influential species and elementary steps via accurately computed DRCs, especially in the transient, can thus aid reaction optimization and mechanism elucidation [20], catalyst screening [17,18], and even development of reduced models for complex reaction systems [42,43].

Overall, in this work, we present a mathematical proof, devoid of any assumption for the overall rate expression, that the summation of the degrees of rate control of all states (intermediates and transition states) is equal to zero. Furthermore, we prove that under SS conditions, the sum of the kinetic degrees of the rate control of all elementary steps (transition states) in a catalytic cycle is conserved at unity, and consequently, the summation of the thermodynamic degrees of rate control for all intermediates is equal to −1. Finally, by utilizing the AD-driven direct sensitivity analysis, we affirm that the above conservations hold true for a relatively complex ethane hydrogenolysis reaction model on Pt (111). Here, we also benchmark the performance of the AD-driven method against the numerical FD technique under both TR and SS reaction conditions. We show that under TR reaction conditions, the sum of the degrees of rate control and the sum of the thermodynamic degrees of rate control do not have to add to 1 and −1, respectively. Very large values are possible with potential consequences for the emerging field of dynamic catalysis and programmable catalysts, i.e., small modifications in a rate-controlling state can lead to dramatic changes in the observed overall reaction rate at transient conditions.

2. Conservation of X_{KRC} and X_{TRC}

2.1. Summation over all degrees of rate controls

The total differential of a function, f, of an array of variables, $\vec{x} = [x_1, x_2, x_3, \cdots, x_n]$, is defined by the following expression:

$$\mathrm{d}f(\vec{x}) = \sum_i^n \left.\frac{\partial f(\vec{x})}{\partial x_i}\right|_{x_{j\neq i}} \bullet \mathrm{d}x_i \tag{3}$$

where, $\left.\frac{\partial f(\vec{x})}{\partial x_i}\right|_{x_{j\neq i}}$ is the partial derivative of the function, $f(\vec{x})$, with respect to x_i, holding other arguments constant.

At constant temperature and partial pressures/activities, the net rate of a network of surface reactions is a function of the free energies of all intermediates (including the catalyst free site or slab) and transition states. If we assume our function is the natural logarithm of the overall reaction rate, ln$r$, and our variables are the dimensionless standard-state free energies of the intermediate and transition states (i.e. $\frac{-G_i^0}{RT}$ for intermediate i and $\frac{-G_j^\ddagger}{RT}$ for transition state j), analogous to eq. 3, the following expression holds for the rate of production of fluid species k in the reaction network:

$$\mathrm{d}(\ln r_{k,fluid}) = \sum_i^l \left.\frac{\partial(\ln r_{k,fluid})}{\partial\left(\frac{-G_i}{RT}\right)}\right|_{G_{j\neq i},T,P_i} \bullet \mathrm{d}\left(-\frac{G_i}{RT}\right) \tag{4}$$

where, l is the sum of the numbers of transition states, m, and intermediates (free site/slab included), n. This implies that the total derivative of the turn-over frequency (TOF) is a sum over the partial derivatives with respect to transition state energies of m elementary reaction steps and the ground state energies of n intermediates (clean catalyst slab/site included). Without lack of generality, we work in the following with the rate, r, instead of the rate of production of fluid species k, $r_{k,fluid}$, although the result is the same for the rate of production of a species.

Rearranging eq. 4 and separating all free energies of transitions states and stable intermediates we can re-express it as:

$$\mathrm{d}(\ln r) = \left[\sum_j^m \left.\frac{\partial(\ln r)}{\partial\left(\frac{-G_j^\ddagger}{RT}\right)}\right|_{G_{k\neq j}^\ddagger, G_i^0, T, P_i} \bullet \mathrm{d}\left(\frac{-G_j^\ddagger}{RT}\right)\right] + \left[\sum_i^n \left.\frac{\partial(\ln r)}{\partial\left(\frac{-G_i^0}{RT}\right)}\right|_{G_{k\neq i}^0, G_j^\ddagger, T, P_i} \bullet \mathrm{d}\left(\frac{-G_j^0}{RT}\right)\right] \tag{5}$$

where $\left.\frac{\partial(\ln r)}{\partial\left(\frac{-G_j^\ddagger}{RT}\right)}\right|_{G_{k\neq j}^\ddagger, G_i^0, T, P_i}$ is the partial derivative of ln$r$ with respect to the dimensionless free energy of the transition state of elementary step j, while the free energy of all other transition states and intermediates are kept constant, and similarly, $\left.\frac{\partial(\ln r)}{\partial\left(\frac{-G_i^0}{RT}\right)}\right|_{G_{k\neq i}^0, G_j^\ddagger, T, P_i}$ is the partial derivative of ln$r$ with respect to the dimensionless free energy of intermediate i, while the free energy of all other transition states and intermediates are constant. We define here the free energy of the transition state as $G_j^\ddagger = G_{j,reac}^0 - RT\ln\left(\frac{k_{f,j}h_p}{k_B T}\right)$, where h_p and k_B are the Planck and Boltzmann constants, respectively, $k_{f,j}$ is the forward rate constant of step j, and $G_{j,reac}^0$ is the free energy of the reactant state of step j (which could involve multiple surface species), i.e., the free energy of the transition state is defined even for reactions with significant tunneling contributions or transmission coefficients smaller one. Also, if the activation free energy barrier, $\Delta G_j^\ddagger$, is coverage dependent, e.g., a linear function in coverage, θ_l: $\Delta G_j^\ddagger = G_j^\ddagger - G_{j,reac}^0 + \sum_l \alpha_{jl}\theta_l$, we obtain $G_j^\ddagger = G_{j,reac}^0 -$

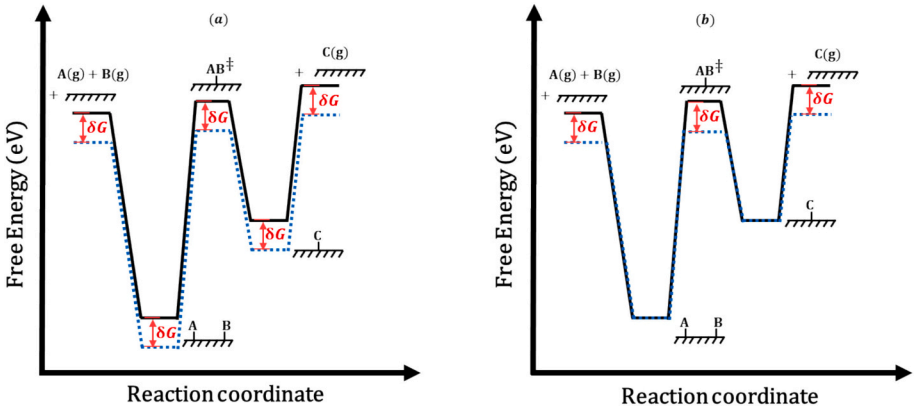

Fig. 1. A schematic of a mechanism, where in (a) all states (intermediates and transition states) are stabilized by δ*G*, and in (b) just the transition states a stabilized by δ*G* while the free energy of all other states remains the same.

$RTln\left(\frac{k_{f,j}h_p}{k_BT}\right) - \sum_l \alpha_{jl}\theta_l$. Now, assuming we stabilize or destabilize all intermediates and transition states uniformly by a constant variation in *G*, *δG*. The elementary reaction free energies and barriers, and consequently elementary forward, backward, and equilibrium rate constants, as well as the TOF, remain unchanged (a schematic of this is shown in Fig. 1a for a typical Langmuir-Hinshelwood mechanism). This is a consequence of the free energy being a state function and the zero of energy being arbitrary. Also, for an elementary reaction, the number of sites is conserved, i.e., the transition state contains the same number of sites as the reactant and product. In other words, the total differential d(ln*r*), from eq. 5, is equal to zero in a case of constant perturbation in the free energies of transition states and intermediates (which includes the free sites).

$$\mathrm{d}(\ln r) = \left[\sum_j^m \left.\frac{\partial(\ln r)}{\partial\left(\frac{-G_j^{\ddagger}}{RT}\right)}\right|_{G_{k\neq j}^{\ddagger},G_i^0,T,P_i} \bullet \mathrm{d}\left(\frac{-G}{RT}\right)\right] + \left[\sum_i^n \left.\frac{\partial(\ln r)}{\partial\left(\frac{-G_i^0}{RT}\right)}\right|_{G_{k\neq i}^0,G_j^{\ddagger},T,P_i} \bullet \mathrm{d}\left(\frac{-G}{RT}\right)\right] = \mathrm{d}\left(\frac{-G}{RT}\right) \bullet \left[\sum_j^m \left.\frac{\partial(\ln r)}{\partial\left(\frac{-G_j^{\ddagger}}{RT}\right)}\right|_{G_{k\neq j}^{\ddagger},G_i^0,T,P_i} + \sum_i^n \left.\frac{\partial(\ln r)}{\partial\left(\frac{-G_i^0}{RT}\right)}\right|_{G_{k\neq i}^0,G_j^{\ddagger},T,P_i}\right] = 0 \tag{6}$$

We highlight that the statement above is correct not only at SS but also under TR conditions as the zero of energy is arbitrary and does not affect TR behavior. From eqs. 1–2, Campbell's kinetic degree of rate control for elementary step *j* and thermodynamic degree of rate control of intermediate *i* are defined as

$$X_{DKRC,j} = \left.\frac{\partial(\ln r)}{\partial(\ln k_j)}\right|_{k_{i\neq j},K_i,T,P_i} = \left.\frac{\partial(\ln r)}{\partial\left(\frac{-G_j^{\ddagger}}{RT}\right)}\right|_{G_{k\neq j}^{\ddagger},G_i^0,T,P_i} = -RT\left.\frac{\partial(\ln r)}{\partial G_j^{\ddagger}}\right|_{G_{k\neq j}^{\ddagger},G_i^0,T,P_i} \tag{7}$$

$$X_{DTRC,i} = \left.\frac{\partial(\ln r)}{\partial(\ln K_i)}\right|_{k_j,K_{k\neq i},T,P_i} = \left.\frac{\partial(\ln r)}{\partial\left(\frac{-G_i^0}{RT}\right)}\right|_{G_{k\neq i}^0,G_j^{\ddagger},T,P_i} = -RT\left.\frac{\partial(\ln r)}{\partial G_i^0}\right|_{G_{k\neq i}^0,G_j^{\ddagger},T,P_i} \tag{8}$$

and by substituting eqs. 7 and 8 into eq. 6, we observe that the summation of the degrees of kinetic and thermodynamic rate controls is conserved and equal to zero as shown in eq. 9 (since $\mathrm{d}\left(\frac{-G}{RT}\right) = \frac{\delta G}{RT} \neq 0$).

$$\sum_j^m X_{DKRC,j} + \sum_i^n X_{DTRC,i} = 0 \tag{9}$$

Since the degrees of rate control are not dependent on the specific perturbation $\mathrm{d}\left(\frac{-G}{RT}\right)$, or whether all states were perturbed by the same amount, eq. 9 is valid at all conditions and all possible perturbations.

2.2. Summation of all degrees of kinetic rate of control

For a typical reaction mechanism with one rate-determining step (RDS), Campbell [1] posited that the degree of rate control of the RDS is unity, while those of other elementary steps are zero. This implies that the summation of the degrees of rate control of a catalytic cycle is equal to one. Kozuch and Shaik [6], Baranski [21], and Dumesic [13] also showed that the summation of the kinetic degree of the rate control of all of the elementary steps is equal to one for some simple reaction schemes where an expression for the TOF of the overall rate is available; however, there is (in our opinion) no rigorous mathematical proof in the literature for conservation of sum of X_{DKRC} for more general reaction

mechanisms with multiple rate-controlling steps, where an expression for the overall rate is not available (we will discuss in more detail the previous proof from Foley and Bhan [14] in Section S7 of the Supporting Information).

Assuming that we uniformly stabilize all the transition states in a reaction mechanism by δG, as shown in Fig. 1b, while the free energies of all intermediates are held constant. Then, eq. 6 can be simplified at constant temperature and fluid conditions as:

$$\mathrm{d}(\ln r) = \left[\sum_j^m \frac{\partial(\ln r)}{\partial\left(\frac{-G_j^{\ddagger}}{RT}\right)}\bigg|_{G_{k\neq j}^{\ddagger}, G_i^0, T, P_i} \bullet \mathrm{d}\left(\frac{-G}{RT}\right)\right] = \sum_j^m X_{DKRC,j} \bullet \mathrm{d}\left(\frac{-G}{RT}\right) \text{ or}$$

$$\mathrm{d}(\ln r_{k,fluid}) = \left[\sum_j^m \frac{\partial(\ln r_{k,fluid})}{\partial\left(\frac{-G_j^{\ddagger}}{RT}\right)}\bigg|_{G_{k\neq j}^{\ddagger}, G_i^0, T, P_i} \bullet \mathrm{d}\left(\frac{-G}{RT}\right)\right] = \sum_j^m X_{k,DKRC,j} \bullet \mathrm{d}\left(\frac{-G}{RT}\right) \tag{10}$$

The net rate for an elementary surface reaction step, r_j, can be written as

$$r_j = k_{f,j} \bullet \overrightarrow{\Theta}_j(\theta_n, P_n) - k_{b,j} \bullet \overleftarrow{\Theta}_j(\theta_n, P_n) \tag{11}$$

where $k_{f,j}$ and $k_{b,j}$ are the forward and backward rate constants of elementary reaction step j, respectively, and $\overrightarrow{\Theta}_j(\theta_n, P_n)$ and $\overleftarrow{\Theta}_j(\theta_n, P_n)$ are functions of the fluid species activity/partial pressure, P_n, and pseudo-coverages, θ_n, of the intermediate n involved in the elementary reaction step j (we typically use the term pseudo-coverage instead of coverage as it is the number of species n on the surface divided by the total number of surface sites, which can differ from the actual coverage for larger surface species). Typically,

$$k_{f,j} = \frac{k_B T}{h_p}\exp\left(-\frac{G_j^{\ddagger} - G_{j,reac}^0}{RT}\right), k_{b,j} = \frac{k_B T}{h_p}\exp\left(-\frac{G_j^{\ddagger} - G_{j,prod}^0}{RT}\right),$$
$$\overrightarrow{\Theta}_j(\theta_n, P_n) = \prod_n \theta_n^{\alpha_{n,j}} \prod_m P_m^{\alpha_{m,j}}, \quad \overleftarrow{\Theta}_j(\theta_n, P_n) = \prod_n \theta_n^{\beta_{n,j}} \prod_m P_m^{\beta_{m,j}} \tag{12}$$

where $G_{j,prod}^0$ is the free energy of the product state of reaction j; $\alpha_{n,j}$ and $\beta_{n,j}$ are the power indices of the coverage of intermediate n in the forward and backward rates of the reaction j, respectively, and $\alpha_{m,j}$ and $\beta_{m,j}$ are the power indices of the activities/partial pressures of fluid species m in the forward and backward rates of the reaction j, respectively. Importantly, if the activation free energy barrier, $\Delta G_j^{\ddagger}$, is coverage dependent, e.g., $\Delta G_j^{\ddagger} = G_j^{\ddagger} - G_{j,reac}^0 + \sum_l \alpha_{jl}\theta_l$, we put the coverage dependence of the rate constant in the coverage functions $\overrightarrow{\Theta}_j(\theta_n, P_n)$ and $\overleftarrow{\Theta}_j(\theta_n, P_n)$ such that, e.g., $\overrightarrow{\Theta}_j(\theta_n, P_n) = \exp\left(-\frac{\sum_l \alpha_{jl}\theta_l}{RT}\right)\prod_n \theta_n^{\alpha_{n,j}} \prod_m P_m^{\alpha_{m,j}}$. In other words, our rate constants above do not have any coverage dependence but a free energy dependence exactly as shown above, and the $\overrightarrow{\Theta}_j(\theta_n, P_n)$ and $\overleftarrow{\Theta}_j(\theta_n, P_n)$ functions do not have any free energy dependence, i.e., α_{jl} are constant and not functions of the free energies (while it might be considered unrealistic that the α_{jl} are not functions of the free energies/material, the separation of a function in free energy and coverage is essential for the following proof).

Next, *at SS*, the mole balance for any given (surface) intermediate ψ can be written as a linear combination of rates of elementary reaction steps that produce or consume species ψ (we limit ourselves here to catalytic surface reactions or any reaction system where the species balances can be written as below, i.e., there is no IN or OUT term but rate of production of species ψ, $r_{\psi,prod}$, is zero).

$$\frac{d\theta_\psi}{dt} = 0 = r_{\psi,prod} = \sum_j^R \nu_{\psi,j} \bullet r_j = \sum_j^R \nu_{\psi,j} \bullet \left[k_{f,j} \bullet \overrightarrow{\Theta}_j(\theta_n, P_n) - k_{b,j} \bullet \overleftarrow{\Theta}_j(\theta_n, P_n)\right] =$$
$$\sum_j^R \nu_{\psi,j} \bullet k_{f,j} \bullet \overrightarrow{\Theta}_j(\theta_n, P_n)\left[1 - \frac{\overleftarrow{\Theta}_j(\theta_n, P_n)}{K_j \bullet \overrightarrow{\Theta}_j(\theta_n, P_n)}\right] \tag{13}$$

where $\nu_{\psi,j}$ is the stoichiometric coefficient of species ψ in elementary reaction j and $K_j = \exp\left(\frac{-\Delta G_j^{rxn}}{RT}\right)$ is the equilibrium constant of elementary reaction j with the free energy of reaction given by $\Delta G_j^{rxn} = G_{j,prod}^0 - G_{j,reac}^0 = \sum_i^{species} \nu_{i,j} G_i^0$. In the case of coverage-dependent reactant free energies, the free energy can usually be split into a coverage-independent part and a coverage-dependent part ($G_i^0 + \sum_l \alpha_{il}\theta_l$) and the coverage dependence can again be moved into the $\overrightarrow{\Theta}_j(\theta_n, P_n)$ and $\overleftarrow{\Theta}_j(\theta_n, P_n)$ functions such that the $k_{f,j}$, $k_{b,j}$ and K_j do not possess any coverage dependence. Such decoupling of the free energy is supported by the literature for both adsorbate [44,45] and transition state binding energies [46,47].

By solving the system of nonlinear differential equations to SS (or solving the nonlinear algebraic equations) resulting from the mole balance for all intermediates and free surface site, we can calculate the coverages of all intermediates and subsequently, the rate of production of any fluid species, k.

$$r_{k,fluid} = \sum_j^R \nu_{k,j} \bullet r_j \tag{14}$$

Upon uniform stabilization of all the transition states by δG while holding the free energies of all intermediates constant, we can write the mole balance equations at the new condition at constant temperature and fluid conditions as

$$\frac{d\theta'_\psi}{dt} = 0 = r'_{\psi,prod} = \sum_j^R \nu_{\psi,j} \bullet r'_j = \sum_j^R \nu_{\psi,j} \bullet k'_{f,j} \bullet \overrightarrow{\Theta}_j(\theta'_n, P_n)\left[1 - \frac{\overleftarrow{\Theta}_j(\theta'_n, P_n)}{K_j \bullet \overrightarrow{\Theta}_j(\theta'_n, P_n)}\right] \tag{15}$$

where the equilibrium constants K_j remain unchanged, and the forward rate constants change to

$$k'_{f,j} = e^{\left(\frac{\delta G}{RT}\right)} \bullet k_{f,j} \tag{16}$$

Now, if we replace all the $k'_{f,j}$ by eq. 16, we can re-write the system of eq. 15 as

$$\frac{d\theta'_\psi}{dt} = 0 = \sum_j^R \nu_{\psi,j} \bullet r'_j = e^{\left(\frac{\delta G}{RT}\right)} \bullet \sum_j^R \nu_{\psi,j} \bullet k_{f,j} \bullet \overrightarrow{\Theta}_j(\theta'_n, P_n)\left[1 - \frac{\overleftarrow{\Theta}_j(\theta'_n, P_n)}{K_j \bullet \overrightarrow{\Theta}_j(\theta'_n, P_n)}\right] \tag{17}$$

and at SS (and only at SS), we can divide eq. 17 by $e^{\left(\frac{\delta G}{RT}\right)}$, finding that the SS equations for the new coverages θ'_ψ, eq. 18, are equivalent to the SS equations for the old coverages θ_ψ in eq. 13.

$$\frac{d\theta'_\psi}{dt} = 0 = \sum_j^R \nu_{\psi,j} \bullet k_{f,j} \bullet \overrightarrow{\Theta}_j(\theta'_n, P_n)\left[1 - \frac{\overleftarrow{\Theta}_j(\theta'_n, P_n)}{K_j \bullet \overrightarrow{\Theta}_j(\theta'_n, P_n)}\right] \tag{18}$$

In other words, the coverages remain unchanged if all transition states of the surface reactions are stabilized by the same amount.

$$\theta_\psi = \theta'_\psi \tag{19}$$

Hence, the rates of all elementary reaction steps j are accelerated by the same constant amount:

$$r_j^{'} = k_{f,j}^{'} \bullet \overrightarrow{\Theta}_j(\theta_n, P_n)\left[1 - \frac{\overleftarrow{\Theta}_j(\theta_n, P_n)}{K_j \bullet \overrightarrow{\Theta}_j(\theta_n, P_n)}\right] \tag{20a}$$

$$r_j^{'} = e^{\left(\frac{\delta G}{RT}\right)} \bullet \left[k_{f,j} \bullet \overrightarrow{\Theta}_j(\theta_n, P_n)\left(1 - \frac{\overleftarrow{\Theta}_j(\theta_n, P_n)}{K_j \bullet \overrightarrow{\Theta}_j(\theta_n, P_n)}\right)\right] \tag{20b}$$

$$r_j^{'} = e^{\left(\frac{\delta G}{RT}\right)} \bullet r_j \tag{20c}$$

Similarly, at constant temperature and fluid conditions, the rate of reaction or the rate of production of any fluid species k becomes:

$$r^{'}_{k,fluid} = \sum_j^R \nu_{k,j} \bullet r^{'}_j = e^{\left(\frac{\delta G}{RT}\right)} \sum_j^R \nu_{k,j} \bullet r_j = e^{\left(\frac{\delta G}{RT}\right)} \bullet r_{k,fluid} \tag{21}$$

Consequently, the infinitesimal change in the free energy of all transition states will change the $\ln r_k$ by $\frac{\delta G}{RT}$.

$$\mathrm{d}(\ln r_k) = \ln r_k^{'} - \ln r_k = \frac{\delta G}{RT} \tag{22}$$

Hence inserting eq. 21 into eq. 10, we obtain:

$$\begin{aligned} \mathrm{d}(\ln r) &= \frac{\delta G}{RT} = \mathrm{d}\left(\frac{-G}{RT}\right) = \left[\sum_j^m X_{DKRC,j}\right] \bullet \mathrm{d}\left(\frac{-G}{RT}\right) \text{ or} \\ \mathrm{d}\left(\ln r_{k,fluid}\right) &= \frac{\delta G}{RT} = \mathrm{d}\left(\frac{-G}{RT}\right) = \left[\sum_j^m X_{DKRC,j|k}\right] \bullet \mathrm{d}\left(\frac{-G}{RT}\right) \end{aligned} \tag{23}$$

which leads to our desired proof (eq. 24) that the sum of the degrees of rate control is 1 at SS

$$\sum_j^m X_{DKRC,j} = 1 \text{ or } \sum_j^m X_{k,DKRC,j} = 1 \tag{24}$$

We reiterate that beyond the SS condition, we require that the rate of a surface or adsorption/desorption reaction be written as:

$$r_j = A_j \exp\left(-\frac{G_j^{\ddagger} - G_{j,reac}^0}{RT}\right) \bullet \overrightarrow{\Theta}_j(\theta_n, P_n)\left[1 - \frac{\overleftarrow{\Theta}_j(\theta_n, P_n)}{K_j(T) \bullet \overrightarrow{\Theta}_j(\theta_n, P_n)}\right] \tag{25}$$

with A_j being a temperature-dependent preexponential constant of reaction j. We note that the rate expression from collision theory for adsorption processes can also be written as in eq. 25. Furthermore, if our rate expressions need to consider some lateral surface interaction parameters, the sensitivity of the rate expression with respect to the lateral interaction parameters are not necessarily zero and this sensitivity is not included in eq. 24 even though the rate expression can be written as in eq. 25, i.e., the sum of sensitivities of all (dimensionless) parameters does not sum to 1.

2.3. Summation of all degrees of thermodynamic rate of control

We have proven that the summation of all degrees of rate control of transition states and intermediates is zero (eq. 9), and that at SS, all degrees of kinetic rate control of transition states sum up to 1 (eq. 24). Consequently, the sum of thermodynamic degrees of the rate control of reaction intermediates is also conserved and adds up to −1, as long as the conditions from eq. 25 are satisfied.

$$\sum_i^n X_{DTRC,i} = -1 \tag{26}$$

2.4. Sensitivity analysis of a simple Langmuir-Hinshelwood mechanism as case study

The Langmuir-Hinshelwood (L-H) mechanism has been used to explain several concepts in heterogenous catalysis. While Campbell's degree of rate control for elementary reactions was first introduced in his 1994 paper [12], Kozuch and Shaik [6,8] pioneered the study of the effect of intermediate concentration and energetics on the overall rate of reaction. As an extension to Cambell's degree of rate control, Stegelmann and coworkers [2,16] defined the degree of thermodynamic rate control for intermediates, using a simple L-H mechanism, with one rate-determining step and three other quasi-equilibrated adsorption-desorption steps, to elucidate the concept. To demonstrate the conservation of the thermodynamic and kinetic degrees of rate control in a reaction at SS, we will use a similar simple L-H mechanism where all surface adsorbates occupy one-site each.

$A_{(g)} + {}^* \rightleftharpoons A^*$ $\quad (quasi-equilibrium)$ $\quad \#(\text{reaction } 1)$

$B_{(g)} + {}^* \rightleftharpoons B^*$ $\quad (quasi-equilibrium)$ $\quad \#(\text{reaction } 2)$

$A^* + B^* \rightleftharpoons C^* + {}^*$ $\quad (RDS)$ $\quad \#(\text{reaction } 3)$

$C^* \rightleftharpoons C_{(g)} + {}^*$ $\quad (quasi-equilibrium)$ $\quad \#(\text{reaction } 4)$

In the above L-H scheme, the asterisk (*) denotes a free catalyst site, $A_{(g)}, B_{(g)}, C_{(g)}$ denote gas phase species, and A^*, B^*, C^* represent surface-bound intermediates. Applying quasi-equilibrium approximations to adsorption-desorption steps, the overall rate of the mechanism above can be obtained as

$$r = \frac{k_3\left[K_1K_2\left[\frac{p_A}{p^0}\right]\left[\frac{p_B}{p^0}\right] - \frac{1}{K_3K_4}\left[\frac{p_C}{p^0}\right]\right]}{\left[1 + K_1\left[\frac{p_A}{p^0}\right] + K_2\left[\frac{p_B}{p^0}\right] + \frac{1}{K_4}\left[\frac{p_C}{p^0}\right]\right]^2} \tag{27}$$

where k_i and K_i denote the forward rate constant of elementary reaction i and the equilibrium rate constant of elementary step i, respectively; p_i is partial pressure of gas species i, and p^0 is the reference pressure (1 bar).

In the absence of lateral interactions between the adsorbed intermediates, one can show that:

$$X_{DKRC,3} = -RT\frac{\partial(\ln r)}{\partial G_3^{\ddagger}}\bigg|_{G_{i\neq 3}^{\ddagger}, G_i^0} = 1 \tag{28}$$

$$X_{DTRC,A} = -RT\frac{\partial(\ln r)}{\partial G_A^0}\bigg|_{G_{j\neq A}^0, G_j^{\ddagger}} = -\left[\frac{2K_1\left[\frac{p_A}{p^0}\right]}{\left[1 + K_1\left[\frac{p_A}{p^0}\right] + K_2\left[\frac{p_B}{p^0}\right] + \frac{1}{K_4}\left[\frac{p_C}{p^0}\right]\right]}\right] = -2\theta_A \tag{29}$$

$$X_{DTRC,B} = -RT\frac{\partial(\ln r)}{\partial G_B^0}\bigg|_{G_{j\neq B}^0, G_j^{\ddagger}} = -\left[\frac{2K_2\left[\frac{p_B}{p^0}\right]}{\left[1 + K_1\left[\frac{p_A}{p^0}\right] + K_2\left[\frac{p_B}{p^0}\right] + \frac{1}{K_4}\left[\frac{p_C}{p^0}\right]\right]}\right] = -2\theta_B \tag{30}$$

$$X_{DTRC,C} = -RT\frac{\partial(\ln r)}{\partial G_C^0}\bigg|_{G_{j\neq C}^0, G_j^{\ddagger}} = -\left[\frac{\frac{2}{K_4}\left[\frac{p_C}{p^0}\right]}{\left[1 + K_1\left[\frac{p_A}{p^0}\right] + K_2\left[\frac{p_B}{p^0}\right] + \frac{1}{K_4}\left[\frac{p_C}{p^0}\right]\right]}\right] = -2\theta_C \tag{31}$$

$$X_{DTRC,*} = -RT\frac{\partial(\ln r)}{\partial G_*^0}\bigg|_{G_{j\neq *}^0, G_j^\ddagger} = \frac{2\left[K_1\left[\frac{p_A}{p^0}\right] + K_2\left[\frac{p_B}{p^0}\right] + \frac{1}{K_4}\left[\frac{p_C}{p^0}\right]\right]}{\left[1 + K_1\left[\frac{p_A}{p^0}\right] + K_2\left[\frac{p_B}{p^0}\right] + \frac{1}{K_4}\left[\frac{p_C}{p^0}\right]\right]} - 1 \tag{32a}$$

$$X_{DTRC,*} = 2[\theta_A + \theta_B + \theta_C] - 1 = \theta_A + \theta_B + \theta_C - \theta_* \tag{32b}$$

A detailed derivation of eqs. 28–32b can be found in Section S1 of the supporting information. As expected based on the quasi-equilibrium assumption for some elementary reaction steps, we observe that the degree of kinetic rate of control for reaction step 3 is unity, and zero for others. The implication of eqs. 28–32b is that, with the exception of the free sites, the thermodynamic degree of rate control of surface intermediates are typically negative regardless of their magnitudes. On the hand, eq. 32b shows that the thermodynamic degree of rate of control of free sites is often positive which correlates with the general observation that an increase in free sites typically leads to a higher reaction rate.

In addition, the thermodynamic degree of rate control for intermediates A, B, and C are equal to $-2\theta_A$, $-2\theta_B$, and $-2\theta_C$, respectively, corroborating the assertion by Stegelmann and coworkers [2], who suggested that the degree of thermodynamic rate of control for any intermediate ψ can be expressed as a function of its coverage, θ_ψ.

$$X_{TRC,\psi} = -\sigma \bullet \theta_\psi \tag{33}$$

where σ is a multiplier, which they posited as the average number of free sites involved in the rate-limiting step.

In the limiting case where the surface is almost fully covered by a particular intermediate, for instance species A, the surface coverage of the abundant species, θ_A, is approximately 1 and, according to eq. 29, its thermodynamic degree of rate of control yields −2. Since other intermediates are nearly non-existent on the surface, their coverages are approximately 0, and their thermodynamic degree of rate of control are effectively zero. In contrast, the degree of thermodynamic rate of control for the free sites, as obtained from eq. 32b, is +1, satisfying eq. 26, but not satisfying eq. 33.

While σ in the above L-H reaction network is an integer and constant, for more complex reaction networks for which analytical solutions are not obtainable, especially those with multiple RDS to varying degrees, σ can be a real number, expected to be a constant in the absence of numerical noises (see Section 4.2).

3. Sensitivity analysis with automatic differentiation

In the following, we utilized automatic differentiation to numerically prove our mathematical derivations for a realistic chemical reaction system. A brief introduction of automatic differentiation and its modes can be found in Section S2 of the Supporting Information documentation.

The evaluation of sensitivity analysis involves the computation of differentials of m functions with respect to n variables, and as real-life models become large and complex, n becomes significantly larger than m. The reverse mode AD becomes efficient for such cases since the evaluation of all differentials can be performed in m passes. Hence, this work couples the reverse mode AD with direct sensitivity analysis to compute the kinetic and thermodynamic DRC of the industrially relevant ethane hydrogenolysis reaction (EH) over Pt(111) active sites, which has importance for understanding both catalytic alkane cracking and polyethylene hydrogenolysis for plastic upcycling [48–50]. Using this model reaction system, we show by example of a complex computational catalysis system that the overall sum of all the kinetic and thermodynamic degrees of rate control is zero, and that at SS, eqs. 24, 26, and 33 are satisfied. Finally, we demonstrate that under TR conditions, the sum of the kinetic degrees of rate control can be very large, deviating significantly from 1.

3.1. DFT details for the sample reaction system

This work models the detailed deconstruction of ethane by hydrogenolysis on the (111) facet of platinum. The model contains 31 reaction steps, including 26 surface reactions and 5 adsorption-desorption steps. Its 16 reaction intermediates, excluding the free site/slab, run the gamut from adsorbed ethane molecules to surface-bound elemental carbon and hydrogen atoms. The Pt(111) catalyst site model was created according to the methodology of Fricke et al. [51] The density functional theory (DFT) implementation in the version 5.4.4 of the Vienna Ab initio Simulation Package (VASP) was used for the geometric optimization of all reactant, product, intermediate, and transition state species. The electron-exchange correlations were described at the generalized gradient approximation (GGA) level using the Perdew-Burke-Ernzerhof functional [52–54], coupled with dispersion corrections based on the D3-technique [55–57]. DFT optimization parameters and convergence criteria are as described in previous work from the Heyden group [51,58–60]. Comprehensive details of the post-optimization DFT energy processing and first-principles microkinetic modeling of the ethane hydrogenolysis reaction at fixed fluid-phase partial pressures can be found in Section S3.1 of the Supporting Information.

3.2. Sensitivity analysis by automatic differentiation on the microkinetic model integration

The computation of the sensitivity of mean-field microkinetic modeling parameters, such as the degree of thermodynamic and kinetic rate control, is complicated by the absence of analytical expressions for the solutions of the pseudo-coverages, θ_i. Since the time-solution of the pseudo-coverages is dependent on the free energies of adsorbed intermediates and transition states, time and initial value of surface coverages, the microkinetic model equations can be re-expressed as in eq. 34, where $\boldsymbol{M}$ is the appropriate mass matrix of the ODE/DAE system; $\boldsymbol{\theta}$ is the vector of pseudo-coverages of surface-bound intermediates and free sites; $\boldsymbol{G^\ddagger}$ and $\boldsymbol{G^0}$ are the vectors of the free energies of the transition states and intermediates, respectively; and $\boldsymbol{\theta_0}$ is the vector of initial values of the pseudo-coverages. This implies that other macroscopic quantities of interest, such as reaction rates (by extension, turnover frequency) and degrees of rate control, are all functions of the parameters mentioned above. Hence, eqs. 1 and 2 can be simplified into eqs. 35 and 36, respectively. While the other terms of eqs. 35 and 36 are relatively easy to obtain via rigorous calculus achieved by the application of algorithmic differentiation on the model equations, the latter term in the summation, $\frac{\partial\boldsymbol{\theta}}{\partial\boldsymbol{\xi}}$ where $\boldsymbol{\xi} \in \{\boldsymbol{G^\ddagger}, \boldsymbol{G^0}, \boldsymbol{\theta_0}\}$, is not readily available in the absence of analytical expressions for $\boldsymbol{\theta}$.

$$\boldsymbol{M} \bullet \frac{d\boldsymbol{\theta}}{dt} = f\left(t, \boldsymbol{\theta}, \boldsymbol{G^\ddagger}, \boldsymbol{G^0}, \boldsymbol{\theta_0}\right) \tag{34}$$

$$X_{DKRC,j} = -RT\left[\frac{\partial(\ln(TOF))}{\partial G_j^\ddagger}\bigg|_{G_{k\neq j}^\ddagger, \boldsymbol{G^0}, \boldsymbol{\theta}} + \sum_{n=1}^{N}\left[\frac{\partial ln(TOF)}{\partial\theta_n}\right]_{\boldsymbol{G^\ddagger}, \boldsymbol{G^0}, \theta_{k\neq n}} \bullet \left[\frac{\partial\theta_n}{\partial G_j^\ddagger}\right]_{G_{k\neq j}^\ddagger, \boldsymbol{G^0}, \theta_{k\neq n}}\right] \tag{35}$$

$$X_{DTRC,i} = -RT\left[\frac{\partial(\ln(TOF))}{\partial G_i^0}\bigg|_{G^{\ddagger},G^0_{k\neq i},\boldsymbol{\theta}} + \sum_{n=1}^{N}\left[\frac{\partial \ln(TOF)}{\partial \theta_n}\right]_{G^{\ddagger},G^0,\theta_{k\neq n}} \bullet \left[\frac{\partial \theta_n}{\partial G_i^0}\right]_{G^{\ddagger},G^0_{k\neq i},\theta_{k\neq n}}\right] \tag{36}$$

By applying automatic differentiation to the integration of the mean-field microkinetic model's system of ODE, we can construct a composite model consisting of the original model equations and the variational differential equations and solve all the terms concurrently while solving the model itself. This approach is the same as the direct sensitivity analysis method [28]. Lehmann [61] and Willkomm [62] clearly explained the methodology to obtain the derivatives of solutions to ODEs with respect to initial values or some parameters. We adapted this methodology to obtain the derivatives of pseudo-coverages with respect to free energies of adsorbates, transition states, and initial coverage conditions.

Assuming that the total differential of unknown pseudo-coverages, $d\boldsymbol{\theta}$, is exact, we can express the time-dependence of its derivatives with respect to free energies and initial values as:

$$\frac{d}{dt}\left[\frac{d\boldsymbol{\theta}}{d\boldsymbol{G}^{\ddagger}}\right] = \frac{d}{d\boldsymbol{G}^{\ddagger}} f\left(t,\boldsymbol{\theta},\boldsymbol{G}^{\ddagger},\boldsymbol{G}^{\mathbf{0}},\boldsymbol{\theta}_{\mathbf{0}}\right) \tag{37}$$

$$\frac{d}{dt}\left[\frac{d\boldsymbol{\theta}}{d\boldsymbol{G}^{\mathbf{0}}}\right] = \frac{d}{d\boldsymbol{G}^{\mathbf{0}}} f\left(t,\boldsymbol{\theta},\boldsymbol{G}^{\ddagger},\boldsymbol{G}^{\mathbf{0}},\boldsymbol{\theta}_{\mathbf{0}}\right) \tag{38}$$

$$\frac{d}{dt}\left[\frac{d\boldsymbol{\theta}}{d\boldsymbol{\theta}_{\mathbf{0}}}\right] = \frac{d}{d\boldsymbol{\theta}_{\mathbf{0}}} f\left(t,\boldsymbol{\theta},\boldsymbol{G}^{\ddagger},\boldsymbol{G}^{\mathbf{0}},\boldsymbol{\theta}_{\mathbf{0}}\right) \tag{39}$$

where,

$$\frac{d\boldsymbol{\theta}}{d\boldsymbol{\zeta}} = \begin{bmatrix} \frac{\partial\theta_1}{\partial\zeta_1} & \frac{\partial\theta_1}{\partial\zeta_2} & \cdots & \frac{\partial\theta_1}{\partial\zeta_n} \\ \frac{\partial\theta_2}{\partial\zeta_1} & \frac{\partial\theta_2}{\partial\zeta_2} & \cdots & \frac{\partial\theta_2}{\partial\zeta_n} \\ \vdots & \vdots & \ddots & \vdots \\ \frac{\partial\theta_m}{\partial\zeta_1} & \frac{\partial\theta_m}{\partial\zeta_2} & \cdots & \frac{\partial\theta_m}{\partial\zeta_n} \end{bmatrix} \quad \forall \quad \boldsymbol{\zeta} \in \left\{\boldsymbol{G}^{\ddagger},\boldsymbol{G}^{\mathbf{0}},\boldsymbol{\theta}_{\mathbf{0}}\right\} \tag{40}$$

Eqs. 37–39 can be expanded to yield the expressions in eqs. 41–43.

$$\frac{d}{dt}\left[\frac{d\boldsymbol{\theta}}{d\boldsymbol{G}^{\ddagger}}\right] = \frac{\partial \boldsymbol{f}\left(t,\boldsymbol{\theta},\boldsymbol{G}^{\ddagger},\boldsymbol{G}^{\mathbf{0}},\boldsymbol{\theta}_{\mathbf{0}}\right)}{\partial \boldsymbol{G}^{\ddagger}}\bigg|_{\boldsymbol{G}^{\mathbf{0}},\boldsymbol{\theta}} + \left[\frac{\partial \boldsymbol{f}\left(t,\boldsymbol{\theta},\boldsymbol{G}^{\ddagger},\boldsymbol{G}^{\mathbf{0}},\boldsymbol{\theta}_{\mathbf{0}}\right)}{\partial \boldsymbol{\theta}}\right]_{\boldsymbol{G}^{\ddagger},\boldsymbol{G}^{\mathbf{0}}} \bullet \left[\frac{d\boldsymbol{\theta}}{d\boldsymbol{G}^{\ddagger}}\right]_{\boldsymbol{G}^{\mathbf{0}},\boldsymbol{\theta}} \tag{41}$$

$$\frac{d}{dt}\left[\frac{d\boldsymbol{\theta}}{d\boldsymbol{G}^{\mathbf{0}}}\right] = \frac{\partial \boldsymbol{f}\left(t,\boldsymbol{\theta},\boldsymbol{G}^{\ddagger},\boldsymbol{G}^{\mathbf{0}},\boldsymbol{\theta}_{\mathbf{0}}\right)}{\partial \boldsymbol{G}^{\mathbf{0}}}\bigg|_{\boldsymbol{G}^{\ddagger},\boldsymbol{\theta}} + \left[\frac{\partial \boldsymbol{f}\left(t,\boldsymbol{\theta},\boldsymbol{G}^{\ddagger},\boldsymbol{G}^{\mathbf{0}},\boldsymbol{\theta}_{\mathbf{0}}\right)}{\partial \boldsymbol{\theta}}\right]_{\boldsymbol{G}^{\ddagger},\boldsymbol{G}^{\mathbf{0}}} \bullet \left[\frac{d\boldsymbol{\theta}}{d\boldsymbol{G}^{\mathbf{0}}}\right]_{\boldsymbol{G}^{\ddagger},\boldsymbol{\theta}} \tag{42}$$

$$\frac{d}{dt}\left[\frac{d\boldsymbol{\theta}}{d\boldsymbol{\theta}_{\mathbf{0}}}\right] = \left[\frac{\partial \boldsymbol{f}\left(t,\boldsymbol{\theta},\boldsymbol{G}^{\ddagger},\boldsymbol{G}^{\mathbf{0}},\boldsymbol{\theta}_{\mathbf{0}}\right)}{\partial \boldsymbol{\theta}}\right]_{\boldsymbol{G}^{\ddagger},\boldsymbol{G}^{\mathbf{0}}} \bullet \left[\frac{d\boldsymbol{\theta}}{d\boldsymbol{\theta}_{\mathbf{0}}}\right]_{\boldsymbol{G}^{\ddagger},\boldsymbol{\theta}} \tag{43}$$

We recognized that the term $\frac{\partial \boldsymbol{f}\left(t,\boldsymbol{\theta},\boldsymbol{G}^{\ddagger},\boldsymbol{G}^{\mathbf{0}},\boldsymbol{\theta}_{\mathbf{0}}\right)}{\partial \boldsymbol{\theta}}\Big|_{\boldsymbol{G}^{\ddagger},\boldsymbol{G}^{\mathbf{0}}}$ is the Jacobian of the microkinetic model, $\mathbf{J}_f$, and by setting $\boldsymbol{Q}_{\boldsymbol{G}^{\ddagger}} = \frac{d\boldsymbol{\theta}}{d\boldsymbol{G}^{\ddagger}}$; $\boldsymbol{Q}_{\boldsymbol{G}^{\mathbf{0}}} = \frac{d\boldsymbol{\theta}}{d\boldsymbol{G}^{\mathbf{0}}}$; $\boldsymbol{R} = \frac{d\boldsymbol{\theta}}{d\boldsymbol{\theta}_{\mathbf{0}}}$; $\boldsymbol{f}_{\boldsymbol{G}^{\ddagger}} = \frac{\partial \boldsymbol{f}\left(t,\boldsymbol{\theta},\boldsymbol{G}^{\ddagger},\boldsymbol{G}^{\mathbf{0}},\boldsymbol{\theta}_{\mathbf{0}}\right)}{\partial \boldsymbol{G}^{\ddagger}}\Big|_{\boldsymbol{G}^{\mathbf{0}},\boldsymbol{\theta}}$; and $\boldsymbol{f}_{\boldsymbol{G}^{\mathbf{0}}} = \frac{\partial \boldsymbol{f}\left(t,\boldsymbol{\theta},\boldsymbol{G}^{\ddagger},\boldsymbol{G}^{\mathbf{0}},\boldsymbol{\theta}_{\mathbf{0}}\right)}{\partial \boldsymbol{G}^{\mathbf{0}}}\Big|_{\boldsymbol{G}^{\ddagger},\boldsymbol{\theta}}$, we can concisely express eqs. 41–43 as:

$$\frac{d\boldsymbol{Q}_{\boldsymbol{G}^{\ddagger}}}{dt} = \boldsymbol{f}_{\boldsymbol{G}^{\ddagger}} + \mathbf{J}_f \bullet \boldsymbol{Q}_{\boldsymbol{G}^{\ddagger}} \tag{44}$$

$$\frac{d\boldsymbol{Q}_{\boldsymbol{G}^{\mathbf{0}}}}{dt} = \boldsymbol{f}_{\boldsymbol{G}^{\mathbf{0}}} + \mathbf{J}_f \bullet \boldsymbol{Q}_{\boldsymbol{G}^{\mathbf{0}}} \tag{45}$$

$$\frac{d\boldsymbol{R}}{dt} = \mathbf{J}_f \bullet \boldsymbol{R} \tag{46}$$

$\boldsymbol{Q}_{\boldsymbol{G}^{\ddagger}}$, $\boldsymbol{Q}_{\boldsymbol{G}^{\mathbf{0}}}$ and $\boldsymbol{R}$ are $N \times M$, $N \times N$ and $N \times N$ matrices, respectively, where N denotes the length of the vector of pseudo-coverages (original state variables—all surface adsorbates and free site), and M is the number of elementary reaction steps. In addition, $\boldsymbol{f}_{\boldsymbol{G}^{\ddagger}}$ and $\boldsymbol{f}_{\boldsymbol{G}^{\mathbf{0}}}$ have the same sizes as $\boldsymbol{Q}_{\boldsymbol{G}^{\ddagger}}$ and $\boldsymbol{Q}_{\boldsymbol{G}^{\mathbf{0}}}$, respectively. While $\boldsymbol{Q}_{\boldsymbol{G}^{\ddagger}}$ and $\boldsymbol{Q}_{\boldsymbol{G}^{\mathbf{0}}}$ are initialized as zero matrices, $\boldsymbol{R}(t=0)$ is set to the identity matrix of order N. To incorporate eqs. 44–46 into the original differential equations, we cast the 2-D vectors into column vectors, and concatenate the resultant column vectors to the original system of differential equations as in eq. 47, where $\lfloor \boldsymbol{n} \rfloor$ denote the operator that reshapes a 2-dimensional matrix $\boldsymbol{n}$ into to a column vector. At every step in the solution of the composite system in eq. 47, updates to $\boldsymbol{Q}_{\boldsymbol{G}^{\ddagger}}$, $\boldsymbol{Q}_{\boldsymbol{G}^{\mathbf{0}}}$ and $\boldsymbol{R}$ require that instantaneous values of $\boldsymbol{f}_{\boldsymbol{G}^{\ddagger}}$, $\boldsymbol{f}_{\boldsymbol{G}^{\mathbf{0}}}$ and $\mathbf{J}_f$ are evaluated. The computation of these 2-dimensional matrices of first-order partial derivatives is performed by incorporating the automatic differentiation implementation in the CasADi [63] software into our microkinetic model. CasADi [63] leverages its symbolic framework to compute analytical differentials, and instant values of differentials are obtained by substituting the variables with their actual values. Additionally, its open-source, plug-and-play nature and easy incorporation into several languages, such as C++, Python, and MATLAB, make it an attractive choice.

$$\boldsymbol{\varphi}' = \begin{bmatrix} \boldsymbol{\theta}' \\ \lfloor \boldsymbol{Q}_{\boldsymbol{G}^{\ddagger}}{}' \rfloor \\ \lfloor \boldsymbol{Q}_{\boldsymbol{G}^{\mathbf{0}}}{}' \rfloor \\ \lfloor \boldsymbol{R}' \rfloor \end{bmatrix} \tag{47}$$

With 17 intermediates (free site included) and 31 elementary reaction steps, the ethane hydrogenolysis system, being studied in this work, yields an augmented system of 1122 differential equations. By solving the augmented system of differential equations and reshaping appropriate subarrays of the dissevered composite vector $\boldsymbol{\varphi}$, we do not only obtain the solution to the pseudo-coverages, $\boldsymbol{\theta}$, but also the numerical values to populate the 2D matrices of $\boldsymbol{Q}_{\boldsymbol{G}^{\ddagger}}$, $\boldsymbol{Q}_{\boldsymbol{G}^{\mathbf{0}}}$, and $\boldsymbol{R}$, simultaneously. The thermodynamic and kinetic degrees of rate of control are then evaluated in vector form as shown in eqs. 48–49, where $\boldsymbol{\eta}^T$ represents the transpose of matrix $\boldsymbol{\eta}$.

Table 1
Steady-state rates of gas-phase production/consumption from the microkinetic model of ethane hydrogenolysis over Pt(111) at 300 °C, 0.13 atm of H_2 and 0.033 atm of CH_3CH_3. Negative values denote net consumption.

S/N	Gas-phase species	Turn-over frequency (TOF) (s^{-1})
1	CH_3CH_3(g)	-7.67×10^{-3}
2	CH_2CH_2(g)	7.67×10^{-3}
3	CHCH(g)	8.03×10^{-15}
4	CH_4(g)	4.34×10^{-7}
5	H_2(g)	7.67×10^{-3}

$$\boldsymbol{X}_{DKRC} = -RT\left[\left.\frac{\partial(\ln(TOF))}{\partial \boldsymbol{G}^{\ddagger}}\right|_{\boldsymbol{G}^{0},\boldsymbol{\theta}} + \boldsymbol{Q}_{\boldsymbol{G}^{\ddagger}}^{T} \bullet \left[\frac{\partial ln(TOF)}{\partial \boldsymbol{\theta}}\right]_{\boldsymbol{G}^{\ddagger},\boldsymbol{G}^{0}}\right] \quad (48)$$

$$\boldsymbol{X}_{DTRC} = -RT\left[\left.\frac{\partial(\ln(TOF))}{\partial \boldsymbol{G}^{0}}\right|_{\boldsymbol{G}^{\ddagger},\boldsymbol{\theta}} + \boldsymbol{Q}_{\boldsymbol{G}^{0}}^{T} \bullet \left[\frac{\partial ln(TOF)}{\partial \boldsymbol{\theta}}\right]_{\boldsymbol{G}^{\ddagger},\boldsymbol{G}^{0}}\right] \quad (49)$$

Unlike the $\boldsymbol{f}_{G^{\ddagger}}$, $\boldsymbol{f}_{G^{0}}$ and $\mathbf{J}_{f}$ above, the $\left.\frac{\partial(\ln(TOF))}{\partial \boldsymbol{G}^{\ddagger}}\right|_{\boldsymbol{G}^{0},\boldsymbol{\theta}}$, $\left.\frac{\partial(\ln(TOF))}{\partial \boldsymbol{G}^{0}}\right|_{\boldsymbol{G}^{\ddagger},\boldsymbol{\theta}}$, and $\left[\frac{\partial ln(TOF)}{\partial \boldsymbol{\theta}}\right]_{\boldsymbol{G}^{\ddagger},\boldsymbol{G}^{0}}$ are relatively easier to evaluate because they are columns of differentials of a scalar function with respect to $\boldsymbol{G}^{\ddagger}$, $\boldsymbol{G}^{0}$, and $\boldsymbol{\theta}$, respectively. They are evaluated using the reverse mode AD implementation in MATLAB's Deep Learning arrays [64].

4. Results and discussion

The composite microkinetic model was evaluated at 300 °C and H_2 and ethane partial pressures of 0.13 and 0.033 atm, respectively, similar to the reaction conditions used by Cortright et al. [65] In addition, these operating conditions are close to those in other works in the literature [66–70].

4.1. Steady-state coverages and reaction rates

First, to validate the AutoDiff solution, the original microkinetic model, which consisted of 17 differential and algebraic equations of coverages, was solved numerically to SS starting from a clean catalyst state. Fig. S4–1 in the Supporting Information shows the time evolution of the pseudo-coverages of free sites and surface species, and it indicates that the system rapidly reaches a SS in pseudo-coverages. Table S4–1 in the Supporting Information shows the values of the pseudo-coverages and derived true coverages at SS. Under these conditions, the surface becomes primarily covered by hydrogen atoms (92.28 %), $CH_3C(***)$ (4.67 %), and free sites (3.04 %). The results obtained are in close agreement with those reported at similar operating conditions by Kuz'min and Zeigarnik [66].

Table 1, an abridged version of Table S4–2 in the Supporting Information, shows the net rates of feed gas consumption and product formation predicted by the microkinetic model. We reckon that the predicted rate of hydrogenolysis based on the production of methane is about 5 orders of magnitude lower than the ~0.015 (s^{-1}) reported in the

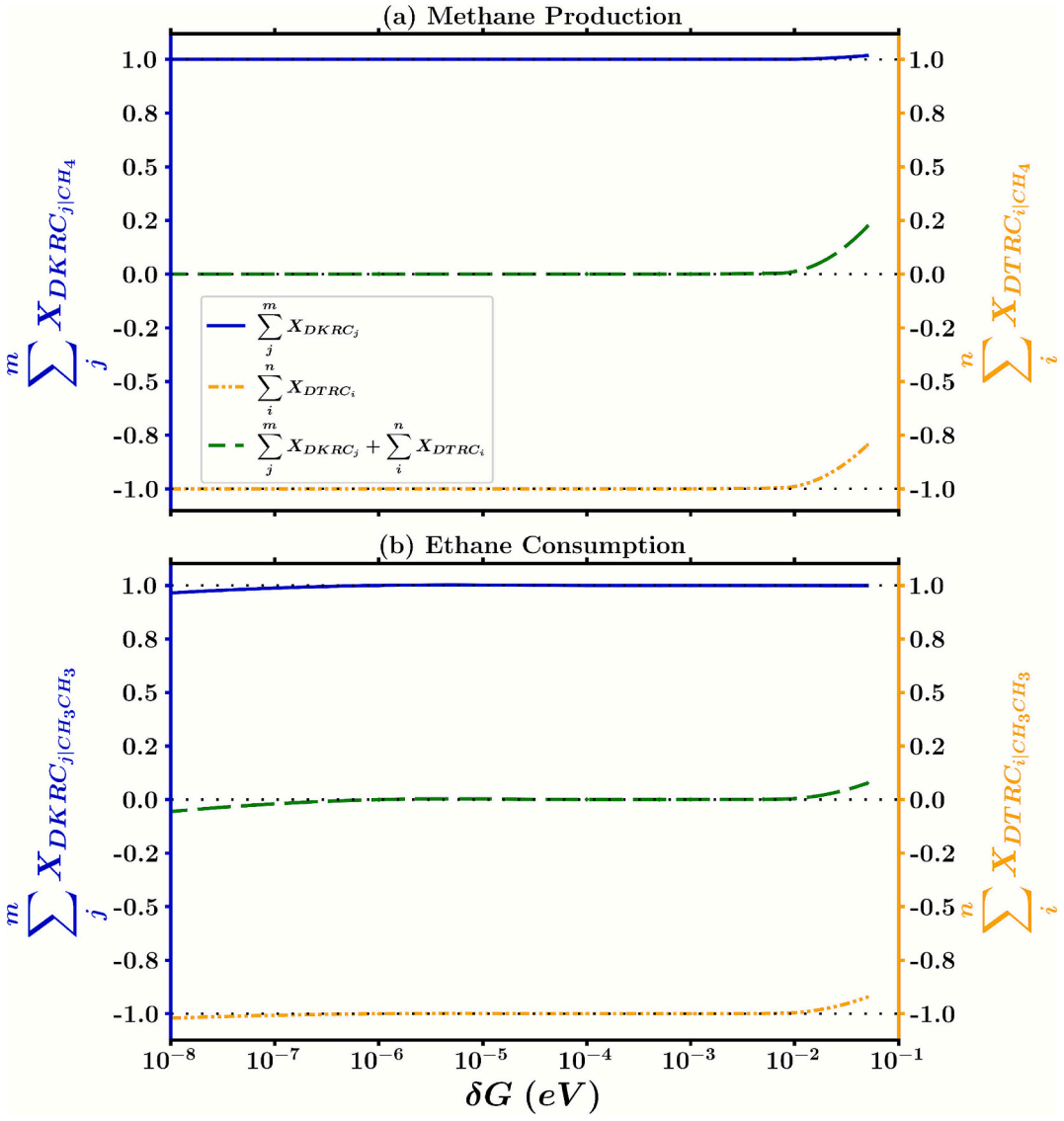

Fig. 2. Effect of energy perturbation size on the sums of sensitivity analysis parameters computed based on a.) methane production rate and b.) ethane consumption rate using the finite difference (FD) approach.

Table 2
Comparison of AD- and FD- derived DTRC ($X_{DTRC,i}$) and sigma (σ_i) values based on methane production.

S/N	Surface species, i	DTRC AD, $X^{AD}_{DTRC,i\|CH_4}$	$\sigma^{AD}_{i\|CH_4} = \frac{-X^{AD}_{DTRC,i\|CH_4}}{\omega_i \bullet \theta_i}$	DTRC FD, $X^{FD}_{DTRC,i\|CH_4}$ ($\delta G = 5 \times 10^{-4}$ eV)	$\sigma^{FD}_{i\|CH_4} = \frac{-X^{FD}_{DTRC,i\|CH_4}}{\omega_i \bullet \theta_i}$
1	CH_3CH_3(*)	-1.240×10^{-4}	3.8791	-1.240×10^{-4}	3.8792
2	CH_3CH_2(*)	-7.369×10^{-5}	3.8791	-7.370×10^{-5}	3.8792
3	CH_3CH(**)	-5.832×10^{-7}	3.8791	-5.832×10^{-7}	3.8792
4	CH_3C(***)	-1.813×10^{-1}	3.8791	-1.813×10^{-1}	3.8792
5	CH_2CH_2(**)	-9.406×10^{-5}	3.8791	-9.406×10^{-5}	3.8792
6	CH_2CH(***)	-3.828×10^{-7}	3.8791	-3.828×10^{-7}	3.8792
7	CH_2C(***)	-1.333×10^{-5}	3.8791	-1.333×10^{-5}	3.8792
8	CHCH(***)	-1.883×10^{-7}	3.8791	-1.883×10^{-7}	3.8792
9	CHC(***)	-3.791×10^{-13}	3.8791	-2.954×10^{-13}	3.0224
10	CC(****)	-3.523×10^{-22}	3.8791	-4.076×10^{-14}	4.4882×10^{8}
11	CH_4(*)	-1.755×10^{-16}	4.3804	-5.237×10^{-14}	1.3074×10^{3}
12	CH_3(*)	-1.355×10^{-12}	3.8790	-1.336×10^{-12}	3.8244
13	CH_2(**)	-1.195×10^{-13}	3.8765	-2.761×10^{-14}	8.9579×10^{-1}
14	CH(***)	-3.895×10^{-10}	3.8793	-3.897×10^{-10}	3.8810
15	C(***)	-1.031×10^{-12}	3.8794	-1.053×10^{-12}	3.9615
16	H(*)	-3.580×10^{0}	3.8791	-3.579×10^{0}	3.8791
17	Free site (*)	2.761×10^{0}	−90.7664	2.761×10^{0}	−90.7662
	$\sum_i^n X_{DTRC,i\|CH_4}$	$\mathbf{-1.000 \times 10^{0}}$		$\mathbf{-1.000 \times 10^{0}}$	

Table 3
Comparison of AD- and FD- derived DTRC ($X_{DTRC,i}$) and sigma (σ_i) values based on ethane consumption.

S/N	Surface species, i	DTRC AD, $X^{AD}_{DTRC,i\|CH_3CH_3}$	$\sigma^{AD}_{i\|CH_3CH_3} = \frac{-X^{AD}_{DTRC,i\|CH_3CH_3}}{\omega_i \bullet \theta_i}$	DTRC FD, $X^{FD}_{DTRC,i\|CH_3CH_3}$ ($\delta G = 10^{-3}$ eV)	$\sigma^{FD}_{i\|CH_3CH_3} = \frac{-X^{FD}_{DTRC,i\|CH_3CH_3}}{\omega_i \bullet \theta_i}$
1	CH_3CH_3(*)	-5.872×10^{-5}	1.8368	-5.873×10^{-5}	1.8371
2	CH_3CH_2(*)	-3.489×10^{-5}	1.8368	-3.494×10^{-5}	1.8391
3	CH_3CH(**)	-2.762×10^{-7}	1.8368	-2.810×10^{-7}	1.8690
4	CH_3C(***)	-8.586×10^{-2}	1.8368	-8.586×10^{-2}	1.8369
5	CH_2CH_2(**)	-4.454×10^{-5}	1.8368	-4.459×10^{-5}	1.8387
6	CH_2CH(***)	-1.813×10^{-7}	1.8368	-1.873×10^{-7}	1.8983
7	CH_2C(***)	-6.312×10^{-6}	1.8368	-6.276×10^{-6}	1.8261
8	CHCH(***)	-8.914×10^{-8}	1.8368	-1.873×10^{-7}	3.8600
9	CHC(***)	-1.795×10^{-13}	1.8368	-9.367×10^{-8}	9.5846×10^{5}
10	CC(****)	-1.668×10^{-22}	1.8368	-2.995×10^{-14}	3.2976×10^{8}
11	CH_4(*)	-7.358×10^{-17}	1.8368	9.367×10^{-8}	-2.3382×10^{9}
12	CH_3(*)	-6.418×10^{-13}	1.8368	9.367×10^{-8}	-2.6808×10^{5}
13	CH_2(**)	-5.662×10^{-14}	1.8368	9.367×10^{-8}	-3.0388×10^{6}
14	CH(***)	-1.844×10^{-10}	1.8368	-9.367×10^{-8}	9.3295×10^{2}
15	C(***)	-4.880×10^{-13}	1.8368	2.879×10^{-15}	-1.08×10^{-2}
16	H(*)	-1.695×10^{0}	1.8368	-1.695×10^{0}	1.8367
17	Free site (*)	7.809×10^{-1}	−25.6712	7.809×10^{-1}	−25.6706
	$\sum_i^n X_{DTRC,i\|CH_3CH_3}$	$\mathbf{-1.000 \times 10^{0}}$		$\mathbf{-1.000 \times 10^{0}}$	

literature [65,71]. This difference originates likely from the importance of other active sites, such as step sites, uncertainties in DFT energies, and the absence of lateral interactions in our model, which leads to excessive hydrogen poisoning [50,60].

4.2. Steady-state sensitivity analysis results

Next, we solved the composite model for the ethane hydrogenolysis reaction network, consisting of 1122 differential and algebraic equations, to SS, which also populates the $\boldsymbol{Q}_{G^i}$, $\boldsymbol{Q}_{G^0}$ and $\boldsymbol{R}$ matrices, which are used to compute the thermodynamic and kinetic degrees of rate control according to eqs. 48–49. To fully understand the advantages of AD relative to a numerical finite difference (FD) calculation of the degrees of rate control for a practical computational catalysis microkinetic model, we also computed the degrees of rate control using a three-point centered FD approach with varying magnitudes of the free energy perturbation, δG. Tables S5–1 and S5–2 in the Supporting Information detail the degrees of rate of control of each surface species and elementary steps, respectively, and their sums computed based on the rate of methane production using FD at varying δG. Likewise, Tables S5–3 and S5–4 show the degrees of rate of control of surface species and elementary steps, respectively, and their sums computed based on ethane consumption rate using the FD at varying δG. Tables S6–1, S6–2, S6–3, and S6–4 in the Supporting Information show their respective corresponding AD-derived values at SS.

By comparing the FD-derived degrees of rate control values at varying perturbation size in Tables S5–1 to S5–4 with their corresponding SS AD-derived values, we observed that relatively large δG, i.e. $\delta G > 10^{-2}$ eV, causes significant inaccuracies in the DRC values, especially the large ones (denoting rate controlling steps/species). These inaccuracies, resulting from truncation error due to the large perturbation and nonlinear model response, trickle down to the sums of DRCs and cause significant deviation in expected conservations (eqs. 9, 24 and 26), as can be seen in the case when $\delta G = 0.05$ eV. With smaller perturbations ($10^{-2} \leq \delta G \leq 10^{-4}$ eV), large DRC values are computed more accurately by FD, evident from the close agreement with AD results. Also, the accuracy of intermediate values (as small as 10^{-6}) is often also improved, but such improvements are rare in very small values. On the other hand, very small magnitudes of perturbation often result in inaccurate DRCs, even in relatively large estimates, stemming from round-off errors due to the finite precision with which computer algorithms represent real numbers and perform computations with them [25].

Table 4
Comparison of steady-state AD- and FD- derived DKRC ($X_{DKRC,j}$).

S/N	Elementary reaction step, j	DKRC AD, $X^{AD}_{DKRC,j\|CH_4}$	DKRC FD, $X^{FD}_{DKRC,j\|CH_4}$ ($\delta G = 5\times10^{-4}$ eV)	DKRC AD, $X^{AD}_{DKRC,j\|CH_3CH_3}$	DKRC FD, $X^{FD}_{DKRC,j\|CH_3CH_3}$ ($\delta G = 10^{-3}$ eV)
1	$CH_3CH_3(*) + * \rightleftharpoons 2\ CH_3(*)$	2.908×10^{-8}	2.908×10^{-8}	8.226×10^{-13}	-2.167×10^{-15}
2	$CH_3CH_3(*) + * \rightleftharpoons CH_3CH_2(*) + H(*)$	3.840×10^{-4}	3.840×10^{-4}	4.288×10^{-4}	4.287×10^{-4}
3	$CH_3CH_2(*) + 2* \rightleftharpoons CH_3(*) + CH_2(**)$	2.191×10^{-3}	2.192×10^{-3}	6.195×10^{-8}	-4.066×10^{-14}
4	$CH_3CH_2(*) + 2* \rightleftharpoons CH_3CH(**) + H(*)$	1.643×10^{-3}	1.643×10^{-3}	3.261×10^{-5}	3.260×10^{-5}
5	$CH_3CH_2(*) + 2* \rightleftharpoons CH_2CH_2(**) + H(*)$	2.604×10^{-3}	2.604×10^{-3}	7.513×10^{-3}	7.513×10^{-3}
6	$CH_3CH(**) + 2* \rightleftharpoons CH_3(*) + CH(***)$	2.108×10^{-1}	2.108×10^{-1}	5.956×10^{-6}	5.901×10^{-6}
7	$CH_3CH(**) + 2* \rightleftharpoons CH_3C(***) + H(*)$	4.199×10^{-6}	4.199×10^{-6}	1.080×10^{-7}	9.367×10^{-8}
8	$CH_3CH(**) + 2* \rightleftharpoons CH_2CH(***) + H(*)$	-4.904×10^{-6}	-4.904×10^{-6}	2.476×10^{-6}	2.435×10^{-6}
9	$CH_3C(***) + * \rightleftharpoons CH_3(*) + C(***)$	6.656×10^{-1}	6.656×10^{-1}	1.881×10^{-5}	1.883×10^{-5}
10	$CH_3C(***) + * \rightleftharpoons CH_2C(***) + H(*)$	-1.529×10^{-4}	-1.529×10^{-4}	7.548×10^{-5}	7.540×10^{-5}
11	$CH_2CH_2(**) + 2* \rightleftharpoons 2\ CH_2(**)$	4.936×10^{-6}	4.937×10^{-6}	1.384×10^{-10}	-6.792×10^{-15}
12	$CH_2CH_2(**) + 2* \rightleftharpoons CH_2CH(***) + H(*)$	-1.266×10^{-3}	-1.266×10^{-3}	3.844×10^{-4}	3.844×10^{-4}
13	$CH_2CH(***) + 2* \rightleftharpoons CH_2(**) + CH(***)$	7.553×10^{-6}	7.553×10^{-6}	2.131×10^{-10}	-3.775×10^{-15}
14	$CH_2CH(***) + * \rightleftharpoons CH_2C(***) + H(*)$	-4.321×10^{-5}	-4.321×10^{-5}	2.133×10^{-5}	2.136×10^{-5}
15	$CH_2CH(***) + * \rightleftharpoons CHCH(***) + H(*)$	4.943×10^{-7}	4.943×10^{-7}	1.358×10^{-11}	3.293×10^{-14}
16	$CH_2C(***) + 2* \rightleftharpoons CH_2(**) + C(***)$	7.905×10^{-8}	7.906×10^{-8}	2.231×10^{-12}	-8.078×10^{-15}
17	$CH_2C(***) + * \rightleftharpoons CHC(***) + H(*)$	8.522×10^{-13}	8.673×10^{-13}	1.659×10^{-15}	-9.367×10^{-8}
18	$CHCH(***) + 3* \rightleftharpoons 2\ CH(***)$	1.214×10^{-1}	1.214×10^{-1}	3.425×10^{-6}	3.372×10^{-6}
19	$CHCH(***) + * \rightleftharpoons CHC(***) + H(*)$	7.505×10^{-11}	7.490×10^{-11}	1.806×10^{-13}	9.367×10^{-8}
20	$CHC(***) + 3* \rightleftharpoons CH(***) + C(***)$	7.781×10^{-8}	7.782×10^{-8}	2.196×10^{-12}	-2.133×10^{-14}
21	$CHC(***) + 2* \rightleftharpoons CC(****) + H(*)$	2.014×10^{-25}	1.785×10^{-14}	2.511×10^{-30}	1.002×10^{-14}
22	$CC(****) + 2* \rightleftharpoons 2C(***)$	1.059×10^{-17}	2.506×10^{-13}	2.988×10^{-22}	-5.797×10^{-15}
23	$CH_4(*) + * \rightleftharpoons CH_3(*) + H(*)$	3.669×10^{-12}	3.758×10^{-12}	1.735×10^{-12}	-2.732×10^{-14}
24	$CH_3(*) + 2* \rightleftharpoons CH_2(**) + H(*)$	3.809×10^{-10}	3.810×10^{-10}	1.804×10^{-10}	-1.842×10^{-14}
25	$CH_2(**) + 2* \rightleftharpoons CH(***) + H(*)$	6.386×10^{-12}	6.326×10^{-12}	3.024×10^{-12}	1.205×10^{-14}
26	$CH(***) + * \rightleftharpoons C(***) + H(*)$	1.033×10^{-12}	1.258×10^{-12}	4.864×10^{-13}	-9.367×10^{-8}
27	$CH_3CH_3(g) + * \rightleftharpoons CH_3CH_3(*)$	4.625×10^{-8}	4.625×10^{-8}	4.183×10^{-8}	-1.695×10^{-16}
28	$CH_2CH_2(g) + 2* \rightleftharpoons CH_2CH_2(**)$	-3.168×10^{-3}	-3.168×10^{-3}	9.915×10^{-1}	9.915×10^{-1}
29	$CHCH(g) + 3* \rightleftharpoons CHCH(***)$	-1.746×10^{-13}	-3.947×10^{-13}	1.044×10^{-12}	-9.367×10^{-8}
30	$CH_4(g) + * \rightleftharpoons CH_4(*)$	1.755×10^{-16}	-5.237×10^{-14}	7.658×10^{-17}	9.367×10^{-8}
31	$H_2(g) + 2* \rightleftharpoons 2H(*)$	3.624×10^{-7}	3.624×10^{-7}	2.093×10^{-7}	2.810×10^{-7}
	$\sum_j^m X_{DKRC,j}$	$\mathbf{1.000\times10^{0}}$	$\mathbf{1.000\times10^{0}}$	$\mathbf{1.000\times10^{0}}$	$\mathbf{1.000\times10^{0}}$
	$\sum_i^n X_{DTRC,i} + \sum_j^m X_{DKRC,j}$	$\mathbf{-1.013\times10^{-12}}$	$\mathbf{2.990\times10^{-5}}$	$\mathbf{-6.250\times10^{-9}}$	$\mathbf{4.488\times10^{-5}}$

Fig. 2 shows the effect of perturbation size on the sums of the sensitivity analysis parameters, and it clearly depicts the deviation of the sums of DKRC, DTRC and their aggregate from 1, −1 and 0, respectively, when large and very small (in the case of TOF formulation based on ethane consumption) energy perturbations are used in the sensitivity analysis via the FD method.

Tables 2 and 3 show the comparison between AD- and FD-derived $X_{DTRC,i}$ and σ_i values for the TOF computed based on methane production and ethane consumption, respectively. Table 4 compares their corresponding $X_{DKRC,i}$ values for both formulations of TOF. It is noteworthy that the AD-derived thermodynamic degrees of rate control values in Tables 2 and 3 at SS are negative for all surface species except for the free sites, implying that stabilization of any adsorbate at SS negatively impacts the reaction rate. Conversely, the positive DTRC value for the free site at SS indicates that more free sites will increase the observed reaction rate. In addition, we observed that the ratio of AD-derived $X_{DTRC,i}$ and true-coverages of adsorbates, $\Theta_i = \omega_i \bullet \theta_i$, (excluding free sites) is constant, except for the instance of $CH_4(*)$ in Table 2, and we attribute this outlier to small errors (noise) in the BLAS routines. The uniformity of σ further underpins Stegelmann and Andreasen's [2] expression of $X_{DTRC,i}$ as a product of some negative number and the intermediate's surface coverage, which is always non-negative, as shown in eq. 33. We can further extend the expression to complex reaction systems where adsorbates occupy multiple sites as:

$$X_{TRC,i} = -\sigma \bullet \omega_i \bullet \theta_i \tag{50}$$

where ω_i represents the number of active sites occupied by species i. Consequently, the degree of thermodynamic rate of control of free sites, $X_{TRC,*}$, can be obtained as:

$$X_{TRC,*} = \sigma \bullet (1 - \theta_*) - 1 \tag{51}$$

Tables 2 and 3 further show that, with optimally chosen δG, large FD-derived degrees of rate control values for rate-controlling species are accurate and in agreement with the AD results. However, for small $X_{TRC,i}$ values such accuracy is difficult to attain with FD.

4.3. Transient sensitivity analysis results

While SS studies can help establish reaction rate laws and their dependence on the reactor's operating condition, TR investigations can often help gain mechanistic insight [72–74]. We computed the TR thermodynamic and kinetic degrees of rate control until SS was reached, starting from a clean catalyst surface. Unlike the SS condition, we observed that large and small values are obtainable for sums of thermodynamic and kinetic degrees of rate control under TR conditions; however, the overall sum is approximately zero. Hence, the conservation over all states (ground and transition states), as mathematically shown in Section 2.1, holds true under TR conditions. Tables S6–5 and S6–6 of the Supporting Information documentation show the TR thermodynamic and kinetic degrees of rate control of intermediates and elementary steps, respectively, when the turnover frequency (TOF) is defined in terms of the methane production rate. Similarly, Tables S6–7 and S6–8 of the Supporting Information documentation detail the TR thermodynamic and kinetic degrees of rate control of intermediates and elementary steps, respectively, based on the ethane consumption rate.

From Table S6–5, we observe several surface-bound intermediates, namely, $CH_3CH_3(*)$, $CH_3CH_2(*)$, $CH_4(*)$, $CH_3(*)$, H(*), and free sites, are initially rate controlling, with $X_{DTRC,i|CH_4}$ values of about −1.00 each. This implies that the methane production rate initially largely depends on the free energies of the species listed. As the reaction proceeds, the influence of most of these initial rate controlling species, except H(*) and the free sites, diminishes in significance, and a new species, CH_3C

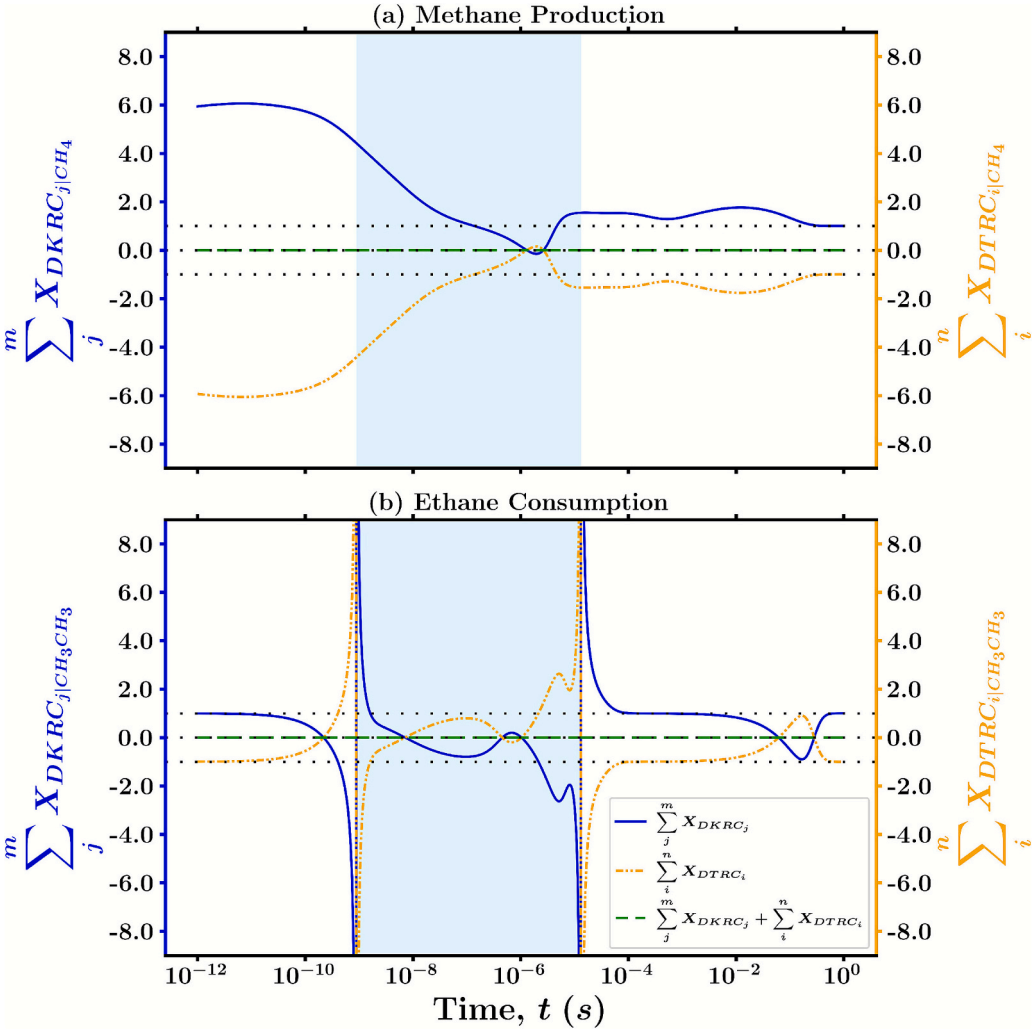

Fig. 3. Sums of transient thermodynamic and kinetic degrees of rate control from AD. These parameters were computed from the microkinetic model based on a.) methane production rate and b.) ethane consumption rate. The shaded region denotes the time range in which the rate of ethane consumption is negative as depicted in Fig. S4–2.

(***), gains somewhat in degree of rate control (SS value of 0.181). This is unsurprising as the CH_3C(***) becomes the most dominant hydrocarbon species on the surface, as shown in Tables S6–1 and S6–3. Furthermore, as the reaction proceeds towards SS, the surface becomes almost entirely covered by adsorbed hydrogen and only relatively few free sites, hence the large $X_{DTRC,i|CH_4}$ values of −3.58 and 2.76 for H(*) and the free site, respectively. Correspondingly, Table S6–6 shows that elementary reaction steps involving early dehydrogenation and C—C bond cleavage are rate controlling, albeit to varying degrees initially and at SS. Namely, elementary adsorption/desorption and initial hydrogenation/dehydrogenation steps 'CH_3CH_3(*) + * ⇌ CH_3CH_2(*) + H(*)', 'CH_3CH_2(*) + 2* ⇌ CH_3(*) + CH_2(**)', 'CH_4(*) + * ⇌ CH_3(*) + H(*)', 'CH_3CH_3(g) + * ⇌ CH_3CH_3(*)', 'CH_4(g) + * ⇌ CH_4(*)' and 'H_2(g) + 2* ⇌ 2 H(*)', have initially $X_{DKRC,j|CH_4}$ values of about 1.00. Though relatively smaller than the aforementioned, reaction steps such as 'CH_3CH_3(*) + * ⇌ 2 CH_3(*)', 'CH_3CH_2(*) + 2* ⇌ CH_3CH(**) + H(*)' and 'CH_3CH(**) + 2* ⇌ CH_3(*) + CH(***)' have non-negligible degrees of rate control values of 0.093, 0.035, and 0.035, respectively. As the reaction proceeds, the influence of most of the major rate controlling steps, formerly mentioned, gradually decline, and some deeper dehydrogenation and C—C cleavage steps, such as 'CH_3CH_2(*) + 2* ⇌ CH_2CH_2(**) + H(*)', 'CH_3CH(**) + 2* ⇌ CH_3C(***) + H(*)', 'CH_3C(***) + * ⇌ CH_3(*) + C(***)', gain in significance for the rate of methane production. Towards SS, only elementary steps involving the cleavage of deeply dehydrogenated C_2H_X species were found to have a significant influence on the rate of methane production, namely, the elementary steps 'CH_3CH(**) + 2* ⇌ CH_3(*) + CH(***)', 'CH_3C(***) + * ⇌ CH_3(*) + C(***)' and 'CHCH(***) + 3* ⇌ 2 CH(***)' with $X_{DKRC,j|CH_4}$ values of 0.211, 0.666, and 0.121, respectively. As expected, the reaction 'CH_3C(***) + * ⇌ CH_3(*) + C(***)' is the dominant rate-controlling step for methane production, since most C—C bond cleavage rate proceeds via the CH_3C(***) intermediate, see Fig. S4–3. Fig. 3 shows the sums of TR $X_{DTRC,i}$ and $X_{DKRC,j}$, and their overall sum, based on methane production and ethane consumptions rates.

As shown in Fig. 3a, unlike the SS case, where all the conservation equations of DRCs derived in Section 2 (eqs. 9, 24, and 26) hold true, in the TR, the individual sums of DKRCs and DTRCs are not conserved at a constant value, and in fact, can be large, small, and even change signs. However, their overall sum, as expressed in eq. 9, is negligible over the entire time range; hence, this conservation holds both in the TR and SS.

Observations from the evaluation of the degrees of rate control based on the rate of ethane consumption, detailed in Tables S6–7 and S6–8, are somewhat different. As shown in Table S6–7, at the onset of the reaction, the free sites and, to a lesser degree, adsorbed ethane, with $X_{DTRC,i|CH_3CH_3}$ values of −1 and 0.004, respectively, are the most rate-controlling species. We highlight the negative degree of rate control for the free site and the positive degrees of rate control for most surface species. As the reaction proceeds with more CH_3CH_3(*) species adsorbed on the

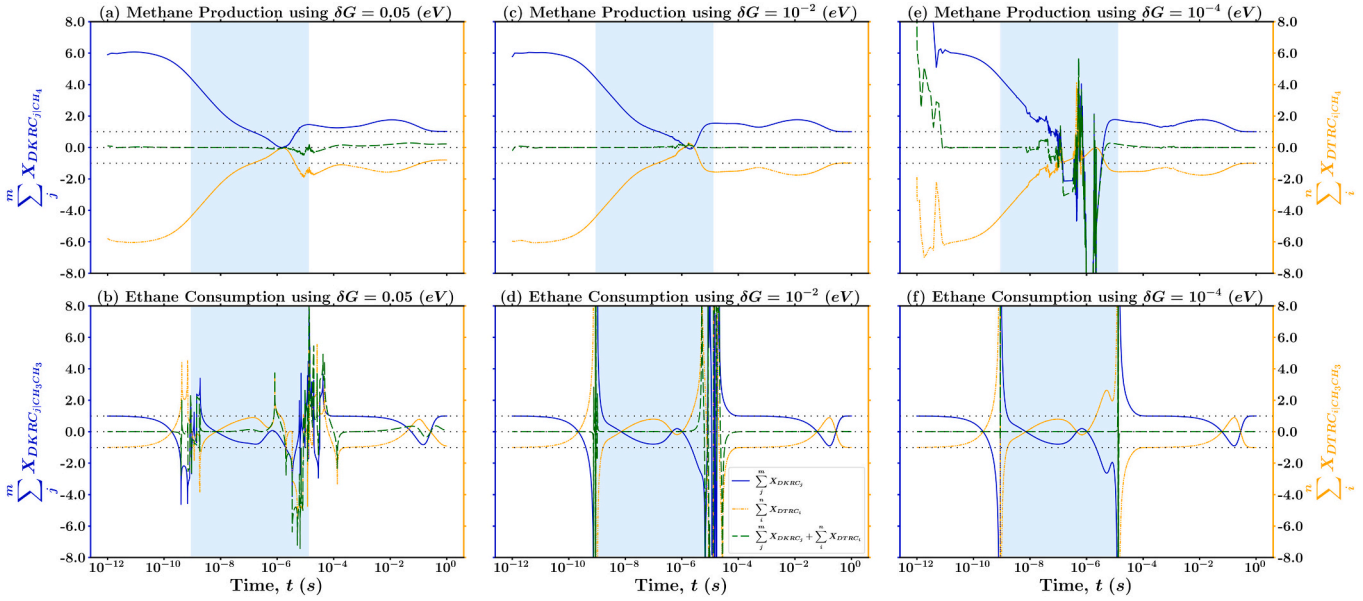

Fig. 4. Sums of transient thermodynamic and kinetic degrees of rate control obtained from finite differences using 3 different sizes of energy perturbation. These parameters were computed from the microkinetic model based on (a) methane production rate using $\delta G = 0.05\ (eV)$, (b) ethane consumption rate using $\delta G = 0.05\ (eV)$, (c) methane production rate using $\delta G = 10^{-2}\ (eV)$, (d) ethane consumption rate using $\delta G = 10^{-2}\ (eV)$, (e) methane production rate using $\delta G = 10^{-4}\ (eV)$, and (f) ethane consumption rate using $\delta G = 10^{-4}\ (eV)$. The shaded region denotes the time range in which the rate of ethane consumption is negative as depicted in Fig. S4–2.

catalyst surface, we observe a short period in which the ethane consumption rate is net negative, as shown in Fig. S4–2. This led to a relatively high positive degree of rate control of the $CH_3CH_3(*)$ species of 1.17 and an overall positive sum of the thermodynamic degree of rate control of 0.166. Beyond the interval of negative ethane consumption, the thermodynamic impact of $CH_3CH_3(*)$ waned, while those of $CH_3C(***)$, H(*), and free sites increased significantly. Towards SS, the $X_{DTRC,i|CH_3CH_3}$ values of surface-bound species slowly become all negative, and only $CH_3C(***)$, H(*), and the free sites remained thermodynamically relevant, with DRC values of −0.086, −1.70, and 0.781, respectively. Similar to the DTRC evaluation based on methane production, H(*) and the free sites had a more significant influence on the rate of ethane consumption, albeit in opposite directions, during the late transient. An inspection of the TR surface coverages reveals that the H(*) coverage increases rapidly from the start of the reaction due to the small H_2 dissociation barrier on Pt, reaching a peak of 96.8 % after approximately 10^{-4} *s*. This high coverage leaves only a few free sites and hydrocarbon species on the surface, and hence, a further increase in H(*) coverage will decrease the reaction rates, as shown by the $X_{DTRC,i|CH_3CH_3}$ values.

For the degrees of kinetic rate control based on ethane consumption detailed in Table S6–8, the adsorption of gas-phase feed molecules, $CH_3CH_3(g)$ and $H_2(g)$, was found to be rate-controlling at the onset of the reaction. As the reaction progressed into the time interval of negative ethane consumption, several early dehydrogenation steps, namely '$CH_3CH_3(*) + * \rightleftharpoons CH_3CH_2(*) + H(*)$', '$CH_3CH_2(*) + 2* \rightleftharpoons CH_3CH(**) + H(*)$', '$CH_3CH_2(*) + 2* \rightleftharpoons CH_2CH_2(**) + H(*)$', become kinetically relevant to the ethane consumption rate, with those leading to the production of $CH_2CH_2(**)$ species having overall a greater positive effect at about 1 μs. The switch to a net positive ethane consumption, at $\sim 10^{-5}$ s, causes a shift in the significance of the elementary reactions; feed adsorption reactions lose influence, and the desorption of the favored product, $CH_2CH_2(g)$, gradually becomes rate-controlling. In addition, although they eventually became relatively kinetically irrelevant at SS, some deeper dehydrogenation steps, such as '$CH_3C(***) + * \rightleftharpoons CH_2C(***) + H(*)$', '$CH_2CH_2(**) + 2* \rightleftharpoons CH_2CH(***) + H(*)$', and '$CH_2CH(***) + * \rightleftharpoons CH_2C(***) + H(*)$', became momentarily rate controlling, albeit, to varying degrees. At SS, the most kinetically crucial reaction steps are '$CH_2CH_2(g) + 2* \rightleftharpoons CH_2CH_2(**)$' and '$CH_3CH_2(*) + 2* \rightleftharpoons CH_2CH_2(**) + H(*)$', having DRCs of 0.992 and 0.008, respectively. Unsurprisingly, no C—C bond-breaking elementary step gained a significant influence on the rate of ethane consumption since the fraction of the total flux of $CH_3CH_3(*)$ adsorbed to C/C cleavage reaction rates is very small. Fig. 3b shows the sums of the TR DKRCs and DTRCs based on ethane consumption. Similar to the previous case of TOF formulation based on methane production, neither the sum of thermodynamic nor kinetic DRC is bounded in the TR state, and sign changes are even observed. However, the overall sum of all thermodynamic and kinetic degrees of rate control is negligible throughout the entire simulation, as stipulated by eq. 9. Lastly, Fig. 3b also shows that at sign changes in ethane consumption rate, the sums of DKRCs and DTRCs are asymptotic and very large numbers, in the thousands, can be obtained, as shown in full-scale graph in Fig. S4–4. Since these sums are almost exact additive inverse each other, the conservation over their overall sum still holds.

Granted, the values obtained for the overall sums of DTRCs and DKRCs in Tables S6–6 and S6–8 are not exact zeros, as prescribed by eq. 9, deviation from zero can be attributed to the rounding error associated with the ANSI/IEEE Standard 754 [75] for binary floating-point arithmetic used in MATLAB to handle fractional number representation [76].

Finally, we evaluated the TR degrees of rate control using finite differences at three different magnitudes of energy perturbation values of 0.05, 10^{-2} and 10^{-4} *eV*. For TOF formulation based on methane production and a step change of 0.05 *eV*, the sums of thermodynamic and kinetic degrees of rate control do not sum to zero even at SS and despite minimal noise in the degree of rate control values, as shown in Fig. 4a. Fig. 4c shows that a perturbation of 10^{-2} *eV* yielded TR and SS sums of thermodynamic and kinetic degrees of rate control that closely mimic the AD results, shown in Fig. 3a, even during TR operation. However, smaller values of δG result in noisy and inaccurate TR sums of thermodynamic and kinetic degrees of rate control, as shown in Fig. 4e. On the other hand, TR sensitivity analysis based on ethane consumption rate shows a different trend. Fig. 4b and d show that perturbations greater than 10^{-4} *eV* evoke a noisy response from the model around time intervals of sign change in ethane consumption. A smaller 10^{-4} *eV*

perturbation yields more accurate results, comparable to the AD-derived values in the TR operation, as shown in Fig. 4f. Hence, a single fixed perturbation may not accurately predict degrees of rate control values for various reaction products in the same reaction system with the FD approach, especially during TR operation.

In general, perturbation size must be carefully chosen with respect to targeted microkinetic model output, especially when computing sensitivities during TR operation—a relatively large perturbation appropriate for a particular targeted output may be too large for another output formulation and cause a nonlinear model response. In addition, excessive reduction in perturbation size does not guarantee a more accurate response due to round-off errors, motivating the use of the AD method.

Finally, in an attempt to reduce the complexity of the composite AD model, we reformulated the AD model without incorporating the $\frac{d\theta}{d\theta_0}$ terms, i.e., the $\boldsymbol{R}$ matrix in eq. 46. Fig. S4–6, juxtaposed with Fig. 3, shows that the incorporation of the $\frac{d\theta}{d\theta_0}$ elements in the AD formulation is only relevant in the TR state (as expected). More details on the importance of the $\frac{d\theta}{d\theta_0}$ matrix can be found in Section S4.2 of the Supporting Information document.

5. Conclusions

A mathematical proof was presented showing that the aggregate sum of the kinetic and thermodynamic degrees of rate control (DRC) equals zero under steady state (SS) and transient (TR) operation. At SS, the sum of kinetic DRCs equals 1, while that of the thermodynamic DRCs equals −1, regardless of the reaction mechanism, conditions, or the turnover frequency definition. Using a Langmuir-Hinshelwood mechanism, we further demonstrated that at SS, the thermodynamic DRCs of surface adsorbates (excluding free sites) are negative and proportional to their surface coverages, a relationship valid for ideal surfaces without lateral interactions.

Then, an Automatic Differentiation-driven (Direct) Sensitivity Analysis technique was developed to accurately compute DRCs, avoiding perturbation errors inherent to finite difference methods. Application to ethane hydrogenolysis confirmed the DRC conservation properties at SS and validated a modified Stegelmann and Andreasen rule for thermodynamic DRCs, $X_{TRC,i} = -\sigma \bullet \omega_i \bullet \theta_i$, which accounts for multisite occupancy.

During TR operation, the sums of the thermodynamic and kinetic DRCs are not bounded: they can assume positive or negative values of varying magnitudes, dictated by the reaction dynamics. Nevertheless, they remain additive inverses of one another. The proposed AD-driven sensitivity framework provides a robust tool for transient catalytic reaction analysis and holds strong potential for advancing research in dynamic catalysis and programmable catalyst design.

CRediT authorship contribution statement

Olajide H. Bamidele: Writing – original draft, Investigation, Formal analysis, Conceptualization. **Sina Behtash:** Writing – review & editing, Investigation, Formal analysis, Conceptualization. **Mubarak Bello:** Writing – review & editing, Investigation, Formal analysis. **Andreas Heyden:** Writing – review & editing, Supervision, Funding acquisition, Formal analysis, Conceptualization.

Declaration of competing interest

The authors declare the following financial interests/personal relationships which may be considered as potential competing interests: Andreas Heyden reports financial support was provided by US Department of Energy. If there are other authors, they declare that they have no known competing financial interests or personal relationships that could have appeared to influence the work reported in this paper.

Acknowledgements

This work has been supported by the Institute for Cooperative Upcycling of Plastics, an Energy Frontier Research Center funded by the U.S. Department of Energy, Office of Science, Basic Energy Sciences, under contract no. DE-AC-02-07CH11358 (Ames National Laboratory). S.B. and A.H. acknowledge financial support from the U.S. Department of Energy, Office of Science, Basic Energy Science under award number DE-SC0007167. The authors also thank Professor Tao Wei of the University of South Carolina, Columbia, for helpful discussions towards this work. Computing resources are provided by the U.S. Department of Energy facility located at the National Energy Research Scientific Computing Center (NERSC) under contract no. DEAC02-05CH11231 and ACCESS facilities located at the Texas Advanced Computing Center, the San Diego Supercomputer Center (SDSC), and Purdue University (grant no. TG-CTS090100). Finally, computing resources provided by the University of South Carolina's High Performance Computing group are gratefully acknowledged.

Appendix A. Supplementary data

Supplementary data to this article can be found online at https://doi.org/10.1016/j.cej.2025.171357.

Data availability

Data will be made available on request.

References

[1] C.T. Campbell, The degree of rate control: a powerful tool for catalysis research, ACS Catal. 7 (2017) 2770–2779. Preprint at, https://doi.org/10.1021/acscatal.7b00115.
[2] C. Stegelmann, A. Andreasen, Finding the key transition states and intermediates controlling net reaction rates and selectivity, Nat. Preced 1–17 (2011), https://doi.org/10.1038/npre.2011.6076.2.
[3] S. Kozuch, J.M.L. Martin, The rate-determining step is dead. Long live the rate-determining state!, ChemPhysChem 12 (2011) 1413–1418.
[4] J.A. Christiansen, The elucidation of reaction mechanisms by the method of intermediates in quasi-stationary concentrations, Adv. Catal. 5 (1953) 311–353.
[5] M. Boudart, Kinetics of Chemical Processes, Prentice-Hall Inc., Englewood Cliffs, NJ, 1968.
[6] S. Kozuch, S. Shaik, A combined kinetic-quantum mechanical model for assessment of catalytic cycles: application to cross-coupling and Heck reactions, J. Am. Chem. Soc. 128 (2006) 3355–3365.
[7] S. Kozuch, S. Shaik, How to conceptualize catalytic cycles? The energetic span model, Acc. Chem. Res. 44 (2011) 101–110.
[8] S. Kozuch, S. Shaik, Kinetic-quantum chemical model for catalytic cycles: the Haber-Bosch process and the effect of reagent concentration, J. Phys. Chem. A 112 (2008) 6032–6041.
[9] M. Boudart, Kinetic generalities in catalysis, Top Catal 14 (2000) 181–185.
[10] J.A. Dumesic, Analyses of reaction schemes using De Donder relations, J. Catal. 185 (1999) 496–505.
[11] C.T. Campbell, Finding the rate-determining step in a mechanism: comparing DeDonder relations with the 'degree of rate control', J. Catal. 204 (2001) 520–524.
[12] C.T. Campbell, Future directions and industrial perspectives micro- and macro-kinetics: their relationship in heterogeneous catalysis, Top. Catal. 1 (1994) 353–366.
[13] J.A. Dumesic, Reply to finding the rate-determining step in a mechanism: comparing dedonder relations with the 'degree of rate control', J. Catal. 204 (2001) 525–529.
[14] B.L. Foley, A. Bhan, Degree of rate control and De Donder relations – an interpretation based on transition state theory, J. Catal. 384 (2020) 231–251.
[15] D.G. Truhlar, W.L. Hase, J.T. Hynes, Current status of transition-state theory, J. Phys. Chem. 87 (1983) 2664–2682.
[16] C. Stegelmann, A. Andreasen, C.T. Campbell, Degree of rate control: how much the energies of intermediates and transition states control rates, J. Am. Chem. Soc. 131 (2009) 8077–8082.
[17] C.A. Wolcott, A.J. Medford, F. Studt, C.T. Campbell, Degree of rate control approach to computational catalyst screening, J. Catal. 330 (2015) 197–207.
[18] W. Yang, et al., Machine learning accelerated first-principles study of the hydrodeoxygenation of propanoic acid, ACS Catal. 14 (2024) 10148–10163.
[19] T. Bligaard, et al., The Brønsted-Evans-Polanyi relation and the volcano curve in heterogeneous catalysis, J. Catal. 224 (2004) 206–217.
[20] C. Stegelmann, N.C. Schiødt, C.T. Campbell, P. Stoltze, Microkinetic modeling of ethylene oxidation over silver, J. Catal. 221 (2004) 630–649.

[21] A. Barański, On the usefulness of Campbell's concept of the rate-determining step, Solid State Ionics 117 (1999) 123–128.
[22] A. Bhan, W.N. Delgass, Best practices in catalysis: a perspective, J. Catal. 405 (2022) 419–429.
[23] B.L. Foley, A. Bhan, Degrees of rate control at non(pseudo)steady-state conditions, ACS Catal. 10 (2020) 2556–2564.
[24] N.K. Razdan, T.C. Lin, A. Bhan, Concepts relevant for the kinetic analysis of reversible reaction systems, Chem. Rev. 123 (2023) 2950–3006.
[25] A.G. Baydin, B.A. Pearlmutter, A.A. Radul, J.M. Siskind, Automatic differentiation in machine learning: a survey, J. Mach. Learn. Res. 18 (2018) 1–43.
[26] Y. Yang, S.K. Achar, J.R. Kitchin, Evaluation of the degree of rate control via automatic differentiation, AICHE J. 68 (2022) 1–9.
[27] J.K. Kim, K. Hur, On the perturbation size of the finite difference method for trajectory sensitivity-based assessment of power system dynamics with non-smooth behavior, Int. J. Electr. Power Energy Syst. 155 (2024) 109647.
[28] A. Sandu, D.N. Daescu, G.R. Carmichael, Direct and adjoint sensitivity analysis of chemical kinetic systems with KPP: part I - theory and software tools, Atmos. Environ. 37 (2003) 5083–5096.
[29] G.I. Marchuk, Adjoint Equations and Analysis of Complex Systems, Springer, Netherlands, Dordrecht, 1995, https://doi.org/10.1007/978-94-017-0621-6.
[30] G.I. Marchuk, V.I. Agoshkov, V.P. Shutyaev, Adjoint Equations and Perturbation Algorithms in Nonlinear Problems, CRC Press, Boca Raton, FL, 1996, https://doi.org/10.1201/9781315136707.
[31] P.J. Dauenhauer, et al., Catalytic resonance theory: parallel reaction pathway control, Chem. Sci. 11 (2020) 3501–3510.
[32] J.G. Patrow, S.A. Sorenson, J.M. Dawlaty, Direct spectroscopic measurement of interfacial electric fields near an electrode under polarizing or current-carrying conditions, J. Phys. Chem. C 121 (2017) 11585–11592.
[33] F. Che, S. Ha, J.S. McEwen, Elucidating the field influence on the energetics of the methane steam reforming reaction: a density functional theory study, Appl. Catal. B 195 (2016) 77–89.
[34] F.A. Garcés-Pineda, M. Blasco-Ahicart, D. Nieto-Castro, N. López, J.R. Galán-Mascarós, Direct magnetic enhancement of electrocatalytic water oxidation in alkaline media, Nat. Energy 4 (2019) 519–525.
[35] M.J. Kale, T. Avanesian, H. Xin, J. Yan, P. Christopher, Controlling catalytic selectivity on metal nanoparticles by direct photoexcitation of adsorbate-metal bonds, Nano Lett. 14 (2014) 5405–5412.
[36] A. Galushko, et al., Introduction to dynamic catalysis and the Interface between molecular and heterogeneous catalysts, in: K. Philoppot, A. Roucoux (Eds.), Nanoparticles in Catalysis: Advances in Synthesis and Applications, WILEY-VCH GmbH, 2021, https://doi.org/10.1002/9783527821761.ch2.
[37] R.M. Choueiri, L.D. Chen, Dynamic control of programmable catalysts offers new dimension for rate enhancement, Chem. Catalysis 2 (2022) 12–15. Preprint at, https://doi.org/10.1016/j.checat.2021.12.021.
[38] M. Shetty, et al., The catalytic mechanics of dynamic surfaces: stimulating methods for promoting catalytic resonance, ACS Catal. 10 (2020) 12666–12695.
[39] R. Imbihl, G. Ertl, Oscillatory kinetics in heterogeneous catalysis, Chem. Rev. 95 (1995) 697–733.
[40] A. Baz, M. Lyons, A. Holewinski, Dynamic electrocatalysis: examining resonant catalytic rate enhancement under oscillating electrochemical potential, Chem. Catalysis 2 (2022) 3497–3516.
[41] P. Jangid, S. Chaudhury, A. Kolomeisky, Theoretical understanding of dynamic catalysis, J. Phys. Chem. C 128 (2024) 9077–9089.
[42] A. Stagni, A. Frassoldati, A. Cuoci, T. Faravelli, E. Ranzi, Skeletal mechanism reduction through species-targeted sensitivity analysis, Combust. Flame 163 (2016) 382–393.
[43] Y. Wu, S. Lin, C.K. Law, B. Yang, Chemical kinetic model reduction based on species-targeted local sensitivity analysis, Int. J. Chem. Kinet. 56 (2024) 445–457.
[44] S.D. Miller, J.R. Kitchin, Relating the coverage dependence of oxygen adsorption on Au and Pt fcc(1 1 1) surfaces through adsorbate-induced surface electronic structure effects, Surf. Sci. 603 (2009) 794–801.
[45] L.C. Grabow, B. Hvolbæk, J.K. Nørskov, Understanding trends in catalytic activity: the effect of adsorbate-adsorbate interactions for Co oxidation over transition metals, Top. Catal. 53 (2010) 298–310.
[46] T. Jiang, et al., Trends in CO oxidation rates for metal nanoparticles and close-packed, stepped, and kinked surfaces, J. Phys. Chem. C 113 (2009) 10548–10553.
[47] H. Falsig, et al., Trends in the catalytic CO oxidation activity of nanoparticles, Angew. Chem. Int. Ed. 47 (2008) 4835–4839.
[48] D.W. Flaherty, E. Iglesia, Transition-state enthalpy and entropy effects on reactivity and selectivity in hydrogenolysis of n -alkanes, J. Am. Chem. Soc. 135 (2013) 18586–18599.
[49] D.W. Flaherty, D.D. Hibbitts, E.I. Gürbüz, E. Iglesia, Theoretical and kinetic assessment of the mechanism of ethane hydrogenolysis on metal surfaces saturated with chemisorbed hydrogen, J. Catal. 311 (2014) 350–356.
[50] M. Bello, B. Rayamajhi, O.H. Bamidele, W. Yang, A. Heyden, Understanding the effect of platinum particle size on ethane dehydrogenation and hydrogenolysis: particle-based microkinetic modeling at finite conversion, ACS Catal. 15 (2025) 12420–12435.
[51] C. Fricke, B. Rajbanshi, E.A. Walker, G. Terejanu, A. Heyden, Propane dehydrogenation on platinum catalysts: identifying the active sites through Bayesian analysis, ACS Catal. 12 (2022) 2487–2498.
[52] J.P. Perdew, K. Burke, M. Ernzerhof, Generalized gradient approximation made simple, Phys. Rev. Lett. 77 (1996) 3865–3868.
[53] J.P. Perdew, Jacob's ladder of density functional approximations for the exchange-correlation energy, in: AIP Conference Proceedings 577, AIP Publishing, 2003, pp. 1–20, https://doi.org/10.1063/1.1390175.
[54] J.P. Perdew, et al., Prescription for the design and selection of density functional approximations: more constraint satisfaction with fewer fits, J. Chem. Phys. 123 (2005).
[55] S. Grimme, J. Antony, S. Ehrlich, H. Krieg, A consistent and accurate ab initio parametrization of density functional dispersion correction (DFT-D) for the 94 elements H-Pu, J. Chem. Phys. 132 (2010), 154104–2.
[56] S. Grimme, S. Ehrlich, L. Goerigk, Effect of the damping function in dispersion corrected density functional theory, J. Comput. Chem. 32 (2011) 1456–1465.
[57] S. Grimme, Density functional theory with London dispersion corrections, WIREs Comput. Mol. Sci 1 (2011) 211–228.
[58] C.H. Fricke, et al., Modeling the effect of surface platinum-tin alloys on propane dehydrogenation on platinum-tin catalysts, ACS Catal. 13 (2023) 10627–10640.
[59] N.A. Szaro, M. Bello, C.H. Fricke, O.H. Bamidele, A. Heyden, Benchmarking the accuracy of density functional theory against the random phase approximation for the ethane dehydrogenation network on Pt(111), J. Phys. Chem. Lett. 14 (2023) 10769–10778.
[60] M. Bello, O.H. Bamidele, G. Terejanu, A. Heyden, Investigation of ethane dehydrogenation and hydrogenolysis on Pt(111), Pt(211), and Pt(100): Bayesian quantification and correction of DFT-based enthalpic and entropic uncertainties, ACS Catal. 15528–15544 (2024), https://doi.org/10.1021/acscatal.4c03455.
[61] L. Lehmann, Derivative of an ODE marching algorithm such as Euler or Runge Kutta, Mathematics Stack Exchange, 2017. https://math.stackexchange.com/questions/2119506/derivative-of-an-ode-marching-algorithm-such-as-euler-or-runge-kutta.
[62] J. Willkomm, Automatic Differentiation of ODE Integration. http://arxiv.org/abs/1802.02247, 2018.
[63] J.A.E. Andersson, J. Gillis, G. Horn, J.B. Rawlings, M. Diehl, CasADi: a software framework for nonlinear optimization and optimal control, Math. Program. Comput. 11 (2019) 1–36.
[64] The MathWorks Inc, Deep Learning Toolbox, Preprint at, https://www.mathworks.com, 2024.
[65] R.D. Cortright, R.M. Watwe, B.E. Spiewak, J.A. Dumesic, Kinetics of ethane hydrogenolysis over supported platinum catalysts, Catal. Today 53 (1999) 395–406.
[66] I.V. Kuz'min, A.V. Zeigarnik, Microkinetic modeling of ethane hydrogenolysis on metals, Kinet. Catal. 45 (2004) 561–569.
[67] G.A. Martin, R. Dutartre, S. Yuan, C. Márquez-Alvarez, C. Mirodatos, Applicability and limits of the ensemble model in catalysis by metals: the kinetics of ethane hydrogenolysis over Pt/SiO2, J. Catal. 177 (1998) 105–112.
[68] J.H. Sinfelt, W.F. Taylor, D.J.C. Yates, Catalysis over supported metals. 111: comparison of metals of known surface area for ethane hydrogenolysis, J. Phys. Chem. 69 (1965) 95–101.
[69] J.H. Sinfelt, D.J.C. Yates, Catalytic hydrogenolysis of ethane over the Noble metals of group VIII, J. Catal. 8 (1967) 82–90.
[70] S.G. Podkolzin, R. Alcala, J.J. De Pablo, J.A. Dumesic, Monte Carlo simulations of reaction kinetics for ethane hydrogenolysis over Pt, J. Phys. Chem. B 106 (2002) 9604–9612.
[71] R.D. Cortright, R.M. Watwe, J.A. Dumesic, Ethane hydrogenolysis over platinum selection and estimation of kinetic parameters, J. Mol. Catal. A Chem. 163 (2000) 91–103.
[72] M.R. Kunz, et al., Data driven reaction mechanism estimation via transient kinetics and machine learning, Chem. Eng. J. 420 (2021) 129610.
[73] Bohdan W. Wojciechowski, Norman M. Rice, Experimental Methods in Kinetic Studies, Elsevier Science, 2003.
[74] C. Waldron, et al., Model-based design of transient flow experiments for the identification of kinetic parameters, React. Chem. Eng. 5 (2020) 112–123.
[75] IEEE Standard for Floating-Point Arithmetic, IEEE Std 754-2019 (Revision of IEEE 754-2008), 2019, pp. 1–84, https://doi.org/10.1109/IEEESTD.2019.8766229.
[76] M.S. Team, How Do I Handle Round-off Errors in My MATLAB Code?. https://www.mathworks.com/matlabcentral/answers/102419-how-do-i-handle-round-off-errors-in-my-matlab-code#answer_111765, 2023.